

FEATURE ARTICLE

[View Article Online](#)
[View Journal](#) | [View Issue](#)

Shape-persistent H-bonded macrocyclic aromatic pentamers[†]

Cite this: *Chem. Commun.*, 2013,
49, 4127

Haoliang Fu,^a Ying Liu^b and Huaqiang Zeng^{*b}

The use of multiple-center intramolecular H-bonds for the efficient construction of macrocycles of varying structures and functions is among the newest and the most noteworthy additions to the toolbox for macrocycle synthesis. This strategy has allowed the creation of sizable interior cavities as small as 2.8 Å and as large as 15 Å in radius in these H-bonded macrocycles with a number of them expressing tailor-made functions. While concentrating on our recent contributions to this fast-growing field, we will further summarize the latest advances on the design, synthesis, structure and function of these shape-persistent H-bonded macrocyclic foldamers that have helped to create a whole new dimension of scientific research, markedly expanding both the structural and functional repertoires of shape-persistent macrocycles.

Received 14th September 2012,
Accepted 10th December 2012

DOI: 10.1039/c2cc36698c

www.rsc.org/chemcomm

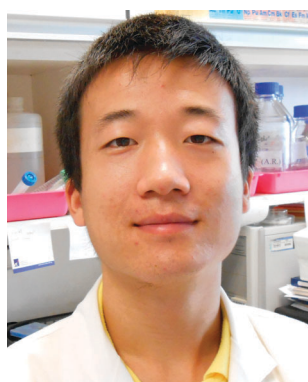
Macrocyclic chemistry is one of the most dynamic and promising frontiers of contemporary chemical research. Researching and identifying new macrocyclic molecules with novel properties therefore have continuously attracted multidisciplinary interests. Yet, critical challenges still remain in the efficient construction of functional macrocycles with precise control over the ring sizes, structures and functions. The recently elaborated shape-persistent

cavity-containing aromatic macrocycles with diverse structures and sizes with rigid, non-collapsible backbones mostly fall within the three general categories, *e.g.*, porphyrin derivatives or analogues,^{1,2} arylene ethynylene macrocycles³ and macrocyclic Schiff bases,^{4,5} exhibiting novel properties with potential for applications in chemistry, materials science, medicine and biology. The shape-persistence and rigidity of these macrocyclic frameworks are largely induced by covalent forces and, to a lesser degree, by built-in H-bonds. The rigidity of macrocyclic frameworks can also arise from the intrinsic conformational bias of the overall backbones⁶ or functional groups such as urea,⁷ amide,^{8–10} or sulfonamide,^{11,12} acting alone, or in a cooperative manner.

^a Faculty of Chemical Engineering and Light Industry, Guang Dong University of Technology, Guang Dong, 510006, China

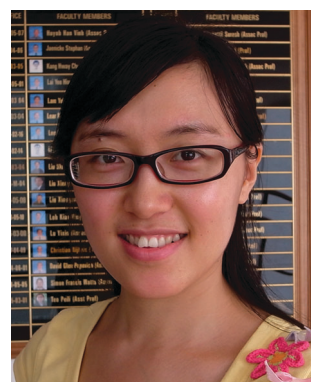
^b Department of Chemistry, National University of Singapore, 3 Science Drive 3, Singapore. E-mail: chmzh@nus.edu.sg; Fax: +65-6779-1691; Tel: +65-6516-2683

† This article is part of the *ChemComm* ‘Emerging Investigators 2013’ themed issue.



Haoliang Fu

Haoliang Fu graduated with a BS in Applied Chemistry with first class honors in 2011. He joined Guangdong University of Technology (GDUT) as a MS student in Applied Chemistry in 2011 and has worked in the laboratory of Professor Kun Zhang at GDUT since July 2011. He is now an exchange student in the laboratory of Professor Huaqiang Zeng at National University of Singapore (NUS). His research interests involve the construction of H-bonded macrocyclic hybrid pentamers as the selective cation receptors.



Ying Liu

cation receptors and as the ligands for the selective recognitions of RNA vs. DNA G-quadruplex structures.

Ying Liu graduated with a BS in Applied Chemistry from Dalian University of Technology in 2007 and a MS in Chemistry from Nanjing University in 2009. She joined the MedChem Programme of NUS Life Sciences as a PhD candidate in January 2009. Currently, she is pursuing graduate studies in the laboratory of Professor Huaqiang Zeng at NUS. Her research interests involve the uses of macrocyclic hybrid pentamers as the selective

A more recent concept regarding the design of sophisticated shape-persistent functional macrocycles explores the proper use of multiply centered intramolecular H-bonding systems to constrain the aromatic backbones^{13–19} and has become a unique way to manipulate an efficient folding of the backbone-rigidified crescent-shaped aromatic foldamers into the corresponding H-bonded macrocyclic structures.^{19,20} Concurrent with the rapid diverse structural elaborations by one-pot H-bonding-assisted macrocyclization,¹⁹ varying functions have also been demonstrated that include selective binding of inorganic^{21–23} and organic²⁴ cations in high affinity, formation of highly conducting transmembrane pores,²⁵ tight associations with neutral molecules such as fullerenes/coronene²⁶ and *p*-toluenesulfonic acid,²⁷ and stabilization of G-quadruplex structures.²⁸

To further expand the structural diversity of H-bonded macrocycles and their potentially realizable functions and applications, we have also reported a series of crescent-shaped or helically folded molecular strands derived from methoxybenzene,^{29–32} pyridone,^{22,33} fluorobenzene^{34,35} and pyridine motifs^{36–41} with their aromatic backbones rigidified by internally placed continuous H-bonding networks. With additional backbone confinement *via* a covalent macrocyclization, the appropriately sized pentamers can become circularly folded to arrive at a unique pentagon shape.^{21,22,31–35} This intrinsic peculiarity requiring five identical repeating units to form a macrocycle is quite unusual and bears few precedents among synthetic foldamers. Except for the Schiff-base macrocycles reported by MacLachlan in 2011,⁴² all the other known H-bonded macrocycles contain no fivefold symmetry. This aesthetically pleasing fivefold symmetry further appears to have been scarcely studied in the hitherto reported shape-persistent macrocycles of varying types. In addition to their unique symmetry, this class of modularly tunable, H-bonded and shape-persistent macrocycles we have developed contain a high degree of precisely tunable interior properties, including effective cavity size, steric crowding, cavity hydrophobicity



Huaqiang Zeng

Huaqiang Zeng received a BS in Chemical Physics from the University of Science & Technology of China (USTC) in 1996 and his PhD from The State University of New York at Buffalo in 2002. After his postdoctoral work with Prof. Peter G. Schultz at The Scripps Research Institute from 2002–2006, he joined the Department of Chemistry at NUS in early July 2006 as an Assistant Professor with a joint appointment in the MedChem Programme of NUS Life Sciences to further his research passions to tackle some challenging issues at the interface of Chemistry and Biology using the knowledge and tools from both Chemistry and Biology.

and cation-binding capacity. A few of these macrocyclic receptors have been demonstrated to be able to selectively recognize specific alkali metal cations with high binding affinities.²¹

1. Evolution of macrocyclic pentamers

The pioneering works exploring the important concept of using a multiple-center H-bonding system to direct the intramolecular folding were carried out by Hamilton and co-workers in 1994,⁴³ focusing on the construction of sheet-like or helical structures such as **1** (Fig. 1a).^{44,45} Although the intramolecular H-bonds of both five and six-membered types found in the 2,6-pyridinedicarboxamide motif could be weak, the formation of such a H-bonding system is favored due to (1) the electrostatic repulsion between the pyridine N-atom and amide O-atom existing in the nearly planar alternative conformations such as **2a** and **2b** shown in Fig. 1b involving a 180° rotation of the amide bond in **1** and (2) a possible existence of a positive cooperativity in forming the three-center H-bonding system, *e.g.*, formation of one intramolecular H-bond energetically increases the bond strength of the other nearby H-bond, and *vice versa*.⁴⁶ In 2000, Gong and co-workers^{47,48} and Lehn and co-workers^{48,49} extended the concept to include the H-bonded oligomeric carboxyamides, respectively, derived from aromatic methoxybenzene (**3** in Fig. 1c) and pyridine motifs (**4** in Fig. 1d).

While Gong's work features readily tunable helical cavities as large as 30 Å in diameter,⁴⁸ Lehn's investigation leads to dynamically formed artificial double-stranded helices, reminiscent of a double-stranded DNA structure.^{49,50} Exploring the same concept, other helically folded structures of varying designs and structures have been recently reported (Fig. 2).^{29,30,38,51–61}

Our analysis of the crystal structures reported by the group of Gong^{47,48} suggested a likelihood for the amide linkages to display a breathing-type behavior in bond angles, resulting in the amide-linked backbone being curved more toward the

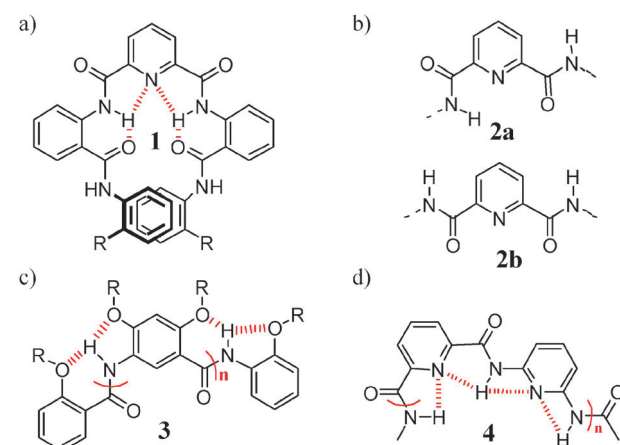


Fig. 1 Structures of (a) a helically folded pyridine-based oligomer **1**, (b) alternative conformations **2a** and **2b** vs. **1**, (c) helically folded methoxybenzene-based foldamers **3** and (d) pyridine-based foldamers **4** that assemble into a double-stranded structure.

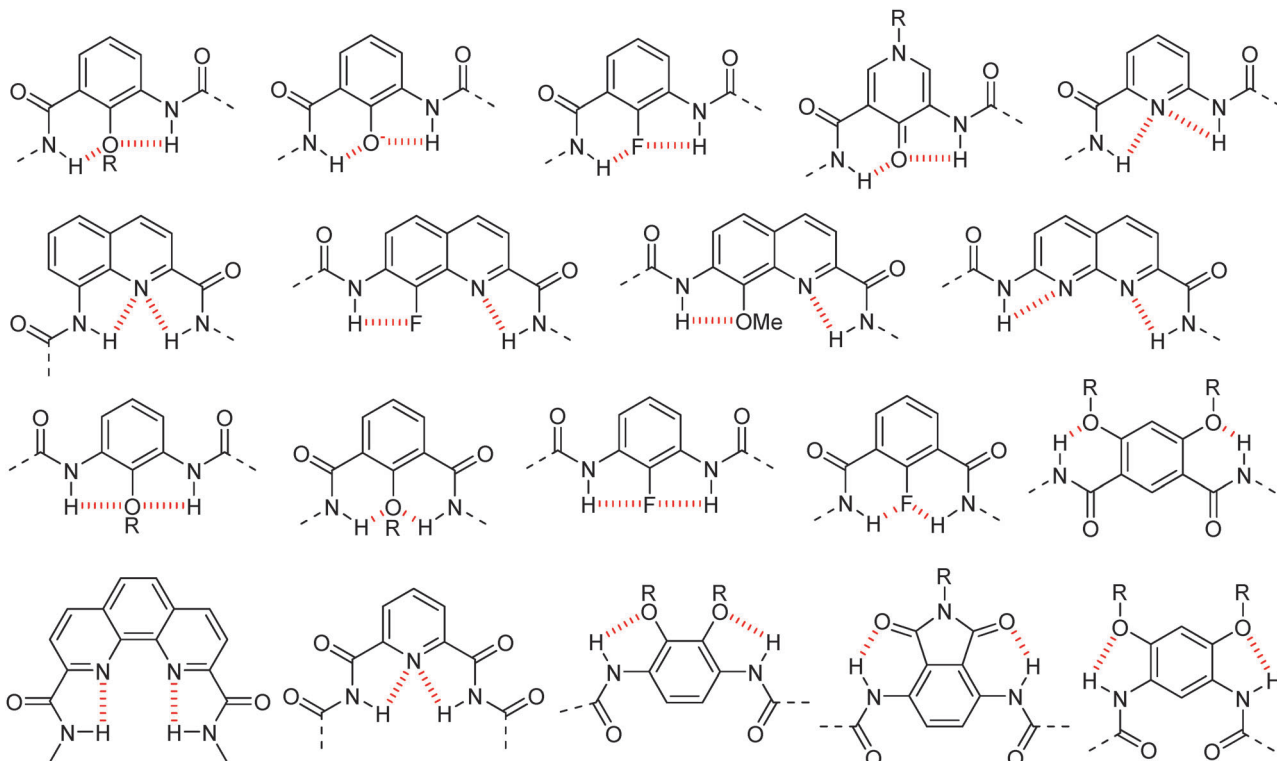


Fig. 2 Other common H-bonding motifs used in the construction of aromatic helices in addition to those in Fig. 1. For a more complete list, see the recent review article by Li and co-workers.¹⁸

H-bonded side. This plasticity in bond angles allows the helices (*e.g.*, 3 in Fig. 1b and its other analogues such as 5 in Fig. 3a) with the H-bonds decorating the exterior of their helical backbones to have ~ 6.5 residues (Fig. 3a), rather than six residues, per helical turn.⁴⁸ This plasticity involving the amide bond can be further substantiated by the *ab initio* calculation at the high level of B3LYP/6-311+G(2d,p).⁶² Computationally, the two highlighted bond angles in dimer 5a deviate from 120° by 2.6° and 8.0° (Fig. 3b), suggesting that the helices derived from this type of building blocks and having the H-bonds around their helical interiors likely require a smaller number of repeating units per

helical turn. As expected, on the basis of these two bond angles, a rough mathematical calculation shows that only five repeating units are needed to form a helical turn if H-bonds are to be located inside the helices. On these grounds, we reasoned that an oligomeric backbone incorporating an inward-pointing, continuous H-bonding network would require about five repeating units per helical turn.³⁰ Consequently, the end-to-end cyclization of a rigidified, crescent acyclic pentamer into a circular form as sketched in circular pentamer 6 might not impose too much angle strain on the molecular backbone and so a planar conformation with a smaller cavity may result. Following this

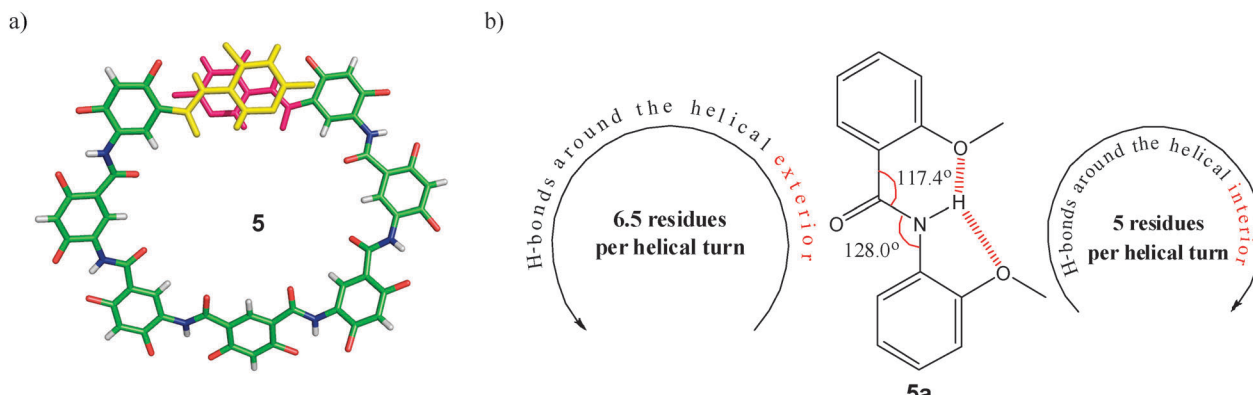
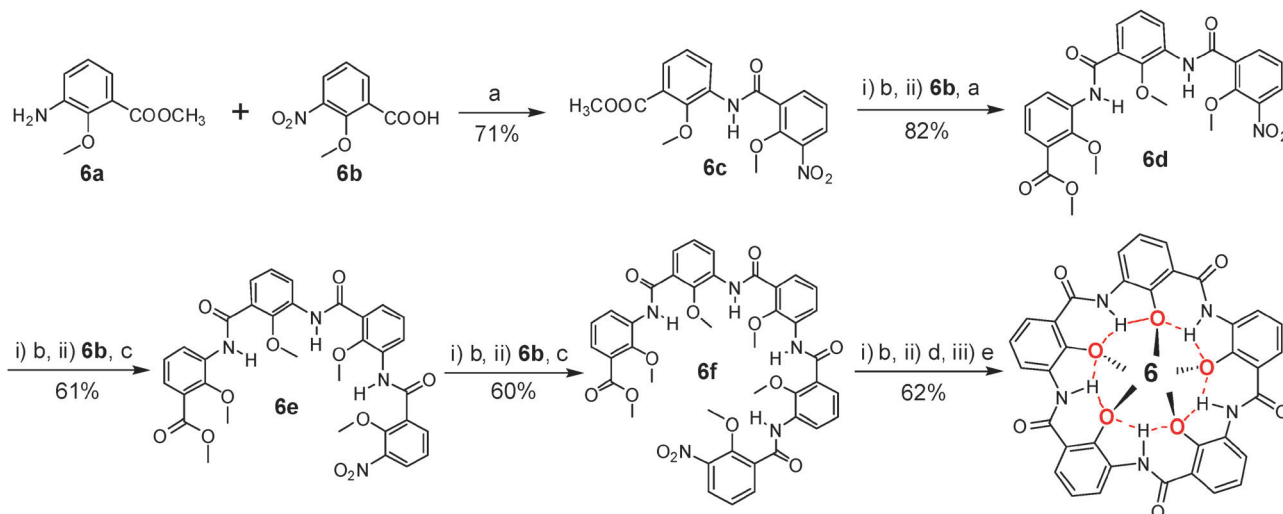


Fig. 3 (a) Top view of the crystal structure of a helically folded symmetric nonamer molecule 5 consisting of one central symmetrical unit and two flanking tetramers that possess ~ 6.5 residues per helical turn.⁴⁸ (b) The bond angles of 117.4° and 128.0° in 5a were determined by the *ab initio* calculation at the B3LYP/6-311+G(2d,p) level. Experimentally, these two angles fall within a range of 116.2° – 117.7° and 126.6° – 128.7° respectively.³⁰ These deviations from 120° make the helical backbone curve more toward the H-bonded side. All the exterior side chains in 5 were removed.



a, ethyl carbonochloridate, 4-methylmorpholine, CH_2Cl_2 , rt, 6 h; b, 20% Pd/C, THF, 40 °C; c, $(\text{COCl})_2$, DMF, TEA, CH_2Cl_2 , 40 °C, 2 h; d, 1M KOH, MeOH, reflux, 2 h; e, BOP, DIEA, CH_2Cl_2 , 2 h

Fig. 4 A stepwise synthetic scheme that leads to pentamer **6** and its other analogues.

speculation, **6** was computationally optimized at the B3LYP/6-31G(d) level,³¹ revealing **6** to adopt an almost flat disk geometry with an appreciable cavity size of 2.85 Å. Using the well established amide coupling methods, **6** was prepared in a stepwise manner (Fig. 4)^{56,63} and its crystal structure pleasantly demonstrates a geometrical shape of a nearly planar pentagon involving five repeating units that are nearly ideally disposed around a rotational axis of C_5 symmetry with internal angles of close to 108° (Fig. 5).³¹ This fivefold folding pattern is quite unusual among all the conformationally defined macrocycles reported to date that have been designed to contain from two to sixfold symmetry.

In the crystal structure of **6**, all the five methoxy oxygen atoms and amide protons point inward and contribute to the formation of a continuous intramolecularly H-bonded network ($\text{NH} \cdots \text{Ome} = 2.2\text{--}2.4$ Å and 1.9–2.0 Å for S(5) and S(6) intramolecular H-bonds, respectively).³¹ The rigidified circular backbone encloses a cavity of 2.85 Å in radius (or 1.45 Å after deducting a covalent radius of 1.4 Å for an oxygen atom) measured from the cavity center to the nucleus of the methoxy O-atoms. This structure also features five methoxy groups spatially arranged in an up-down-up-down-up fashion (Fig. 5b and c). This sequential arrangement turns out to be

the most stable and more stable than other alternative arrangements involving five interior methyl groups by 2.5–7.5 kcal mol⁻¹ at the B3LYP/6-31G(d) level. These alternating methyl groups further form two hydrophobic caps made up of three and two methyl groups, respectively, covering either side of the pentamer plane and completely blocking the cavity. It is also worth pointing out that the X-ray determined structure of **6** is remarkably similar to its *ab initio* calculated structure at the level of B3LYP/6-31G*. This highlights a high applicability and reliability of *ab initio* calculations at the B3LYP/6-31G(d) level to accurately derive the structures of intramolecularly H-bonded aromatic backbones in the absence of crystal structures.

2. Diversifying the structures and functions of macrocyclic pentamers

2.1 Methoxybenzene-based pentamers²¹

One of our initial objectives in designing circularly folded pentamer **6** is to build a cation-binding capacity into its cavity. Although **6** encloses a suitably sized cavity of ~2.85 Å in radius decorated by five convergently aligned O-atoms, the two steric caps comprised of three and two interior methoxy methyl groups, respectively, on either side of the ring plane, completely block the cavity, and prevent metal cations such as Na^+ (~1.0 Å), K^+ (~1.4 Å), etc. from entering it (Fig. 5b and c). Not surprisingly, our numerous attempts to effect the binding of **6** by all the five alkaline metal cations were unsuccessful. Given the fact that the radii of a majority of cations are less than 1.4 Å, the presence of the methyl groups provided us with an efficient means to fine-tune the effective cavity size and hydrophobicity of the ion-binding cavity. We thus envisioned that a stepwise replacement of the interior methyl groups with hydroxyl groups should give rise to varying pentamers **7a**–**7d** with their effective cavities increasingly enlarged (Fig. 6). By converting the phenyl groups into phenolate anions

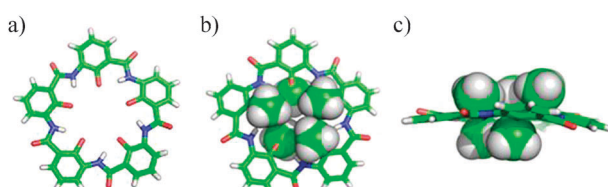


Fig. 5 Crystal structure of macrocyclic pentamer **6**: (a) top view with interior methoxy methyl groups omitted for clarity of view, (b) top and (c) side views of **6** with the methyl groups in CPK representations. The hydrophobic caps made up of methyl groups apparently block the cavity and prevent **6** from binding to metal cations.

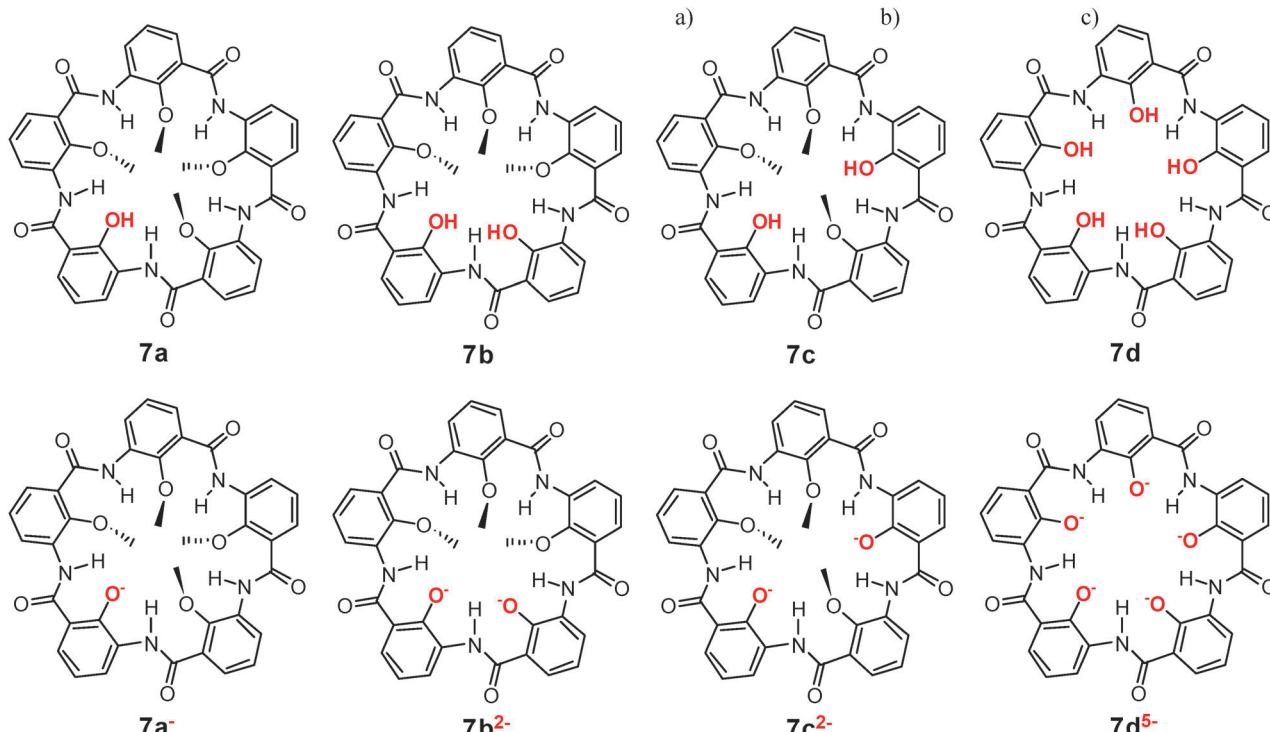


Fig. 6 Structures of hydroxyl-containing circular pentamers **7a–7d**. The corresponding anionic hosts can be generated by deprotonating hydroxyl groups using tetrabutylammonium hydroxide (TBAOH). These pentamers can be similarly made according to the scheme outlined in Fig. 4.

via deprotonation, the cavity in their anionic analogues should be further increased along with their binding affinities. It is our belief that **7b** and **7c** as well as their anionic versions containing two phenol moieties at different locations should also differ in their effective cavity size as methyl groups may have subtly different orientations. As such, these pentamers may display differential binding affinities toward metal ions.

The single crystal structure of **7a** shows that **7a** similarly folds into an almost planar disc arrangement of nearly perfect C_5 symmetry (Fig. 7a). A continuously formed H-bonding network brings the five aryl-bonded oxygens in a circular manner to enclose a cavity of $\sim 2.88 \text{ \AA}$ in radius, nearly identical to that found in **6** (Fig. 5). Two hydrophobic caps comprising four methyl groups and one hydrogen atom are found below and above the plane. This structural study clearly demonstrates that replacing methoxy groups with hydroxyl groups does not interrupt the continuous H-bonding network

nor does it adversely alter the cavity shape and size necessary for efficient cation interactions.

The subsequent determination of the association constants for complexing alkaline metal cations (Li^+ , Na^+ , K^+ , Rb^+ , and Cs^+) by neutral **7a–7c** and anionic **7a–7c²⁻** hosts indeed reveals selective recognitions of metal ions by these pentamers.²¹ Even though none of neutral **7a–7c** and anionic **7a⁻** hosts binds any alkaline metal cation in acetonitrile, anionic hosts **7b²⁻** and **7c²⁻** do exhibit differential bindings toward Na^+ , K^+ , Rb^+ , and Cs^+ (Table 1). While **7b²⁻** binds smaller cations (Na^+ and K^+) more strongly than larger cations (Rb^+ and Cs^+), **7c²⁻** displays a reversed trend in that it tightly binds Rb^+ and Cs^+ , but not Na^+ and K^+ . Thus, a simple separation of the two interior hydroxyl groups with one methoxy group as in **7c** significantly alters its binding profile toward the five alkaline metal cations with respect to **7b²⁻**. This noteworthy difference in binding affinities among anionic **7a⁻**, **7b²⁻** and **7c²⁻** demonstrates that a tunability in interior properties indeed imparts experimentally measurable ion-binding selectivity to the hosts, and fully demonstrates the potential of our system to produce macrocycles with precisely tunable interior chemical and physical properties.

The crystal structures of complexes determined $\text{K}^+@\text{anionic } \mathbf{7b}^{2-}$ and $\text{Cs}^+@\text{anionic } \mathbf{7c}^{2-}$ help provide the structural insights into the origin of selective binding (Fig. 7b and c). In the complex $\text{K}^+@\text{anionic } \mathbf{7b}^{2-}$, K^+ ion is largely stabilized by two strongly-coordinating anionic phenolate O-atoms (K^+-O^- distances = 2.68 and 2.73 \AA) but destabilized by a hydrophobic methyl group ($\text{K}^+-\text{H}-\text{CH}_2\text{O}$ distance = 3.21 \AA). With respect to the position of K^+ in **7b²⁻**, smaller cations such as Li^+

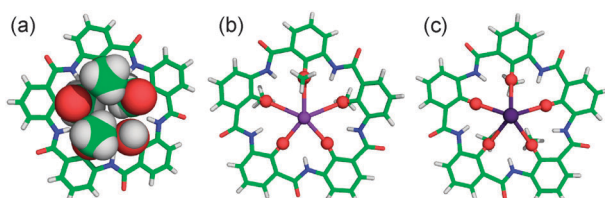


Fig. 7 Top views of the crystal structures of (a) **7a**, (b) the complex $\text{K}^+@\text{anionic } \mathbf{7b}^{2-}$ and (c) the complex $\text{Cs}^+@\text{anionic } \mathbf{7c}^{2-}$. CPK models of methoxy and hydroxyl groups in (a) were built based on the van der Waals radius (gray: $\text{H} = 1.20 \text{ \AA}$; green: $\text{C} = 1.70 \text{ \AA}$; red: $\text{O} = 1.52 \text{ \AA}$, $\text{O}^- = 1.40 \text{ \AA}$). In both (b) and (c), $\text{O} =$ red sphere, $\text{K}^+ =$ purple sphere, $\text{Cs}^+ =$ deep blue sphere.

Table 1 Differential binding affinities^a ($K_a \times 10^{-5}$ M) toward alkaline metal cations (Li^+ , Na^+ , K^+ , Rb^+ , and Cs^+) by anionic hosts **7b**²⁻ and **7c**²⁻ with a 1 : 1 binding stoichiometry

	Li^+	Na^+	K^+	Rb^+	Cs^+
7b ²⁻	16.8/0.15 ^b	1.77 ± 0.38	1.00 ± 0.18	—	—
7c ²⁻	0.85 ± 0.23	—	—	0.12 ± 0.03	0.55 ± 0.16

^a Determined by Isothermal Titration Calorimetry in acetonitrile at 25 °C. ^b 2 : 1 binding stoichiometry for two binding site modes (2 Li^+ @anionic **7b**²⁻) is possible but the uncertainties are greater than the binding constants.

($V_{\text{dW}} = 0.76$ Å) and Na^+ (1.02 Å) can similarly remain in proximity to phenolate O-atoms, forming two strong $\text{M}^+ - \text{O}^-$ coordination bonds that override the destabilization from the adjacent hydrophobic methyl group.⁶⁴ In contrast, larger cations, such as Rb^+ (1.52 Å) and Cs^+ (1.67 Å), are forced into the vicinity of the hydrophobic methyl group, leading to strong repulsions that disallow a concurrent binding of the two phenolate O-atoms. Consequently, no appreciable bindings can be determined for Rb^+ and Cs^+ . In the case of **7c**²⁻, only Rb^+ and Cs^+ can form two strong $\text{M}^+ - \text{O}^-$ coordination bonds ($\text{Cs}^+ - \text{O}^-$ distances = 3.00 and 3.05 Å) that lead to the complex formation, and both Na^+ and K^+ form at most one strong $\text{M}^+ - \text{O}^-$ coordination bond that produces no detectable or very weak bindings.

2.2 Pyridone-based pentamers²²

Due to the stabilization of the phenolate anion *via* the formation of intramolecular H-bonds, the pK_a of the phenolic hydroxyl groups in **7a**–**7c** lowers down to ~8.4, a value that is 1.6 lower than that of the typical phenolic hydroxyl group. This value, however, is still relatively high, and suggests that the phenolate anion in anionic hosts **7b**²⁻ and **7c**²⁻ readily undergoes re-protonation under the physiological conditions at a pH of 7.4. Once re-protonated, these pentamer hosts lose their

ability to tightly bind alkaline metal ions, thereby limiting their potential applications.

To eliminate this undesired attribute associated with the hydroxyl-containing pentamers, an alkylated 4(1H)-pyridone motif was introduced into the pentameric backbone. Acid- and amine-containing alkylated pyridone units **8k** and **8l** take five steps to make with an overall yield of ~12% starting from the commercially available diethyl 3-oxopentanedioate (Fig. 8). By performing a series of iterative couplings using HBTU, followed by a BOP-mediated end-to-end intramolecular cyclization, pentamers **8a**–**8f** carrying varying side chains can be made after 10 more steps with an overall yield of ~1%.⁶⁵

The ability of the interior carbonyl O-atoms to form intramolecular H-bonds (2.00–2.27 Å) with the adjacent amide protons can be demonstrated by the crystal structure of a dimer molecule **8m** (Fig. 9a).²² The formation of these intramolecular H-bonds restricts the conformational freedom of the amide bonds and biases the aromatic backbone into a defined crescent shape. Computations at the B3LYP/6-31G(d) level on the pentamer composed of five pyridone units with or without bound K^+ ion in the center show that such a pentagonal shape encloses a hydrophilic oxygen-containing cavity of 2.85 Å, nearly identical to the average coordination bond distance between K^+ ions and covalently bound O-atoms (Fig. 9b and c). As such, K^+ ion stays in the center of the cavity and remains coplanar with the pentameric plane. As illustrated in Fig. 9d, despite the high quality single crystals obtained for **8a**, its structure could not be confidently determined and fully refined, possibly due to the packing problem by pentagon-shaped molecules.³⁴ Nevertheless, from the partially refined structure, fivefold symmetry and planarity can be clearly seen.

Considering the electron rich nature of the carbonyl O-atom, the five convergently aligned, properly spaced O-atoms should suggest high-affinity cooperative recognition of metal ions by pentameric molecules **8a**–**8f**. A first indication suggesting a good binding of alkali metal ions by **8a**–**8f** came from the

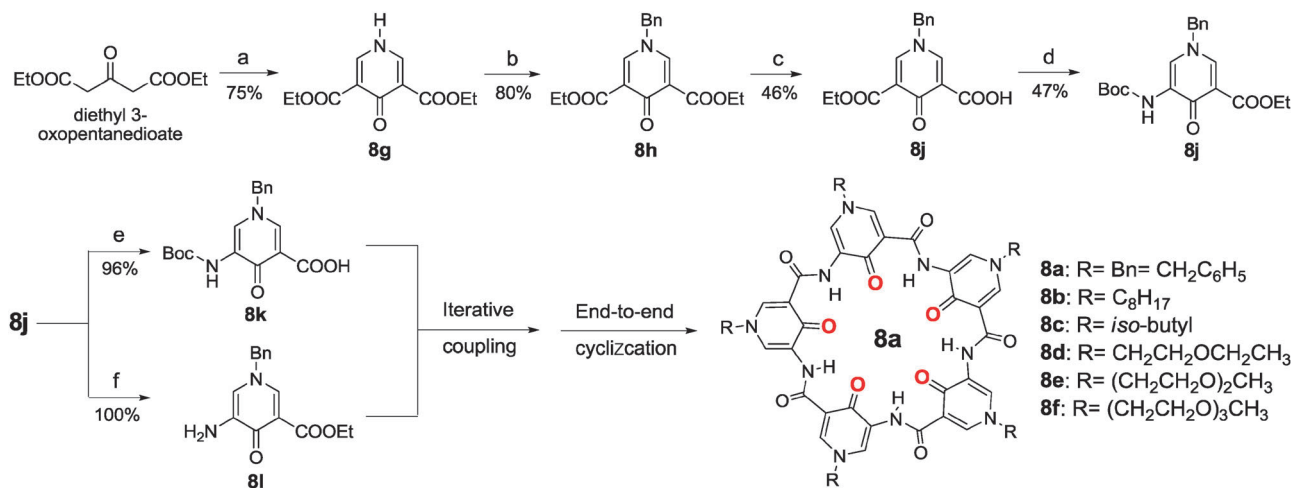


Fig. 8 Exemplified synthesis of monomeric pyridone units **8k** and **8l** used for constructing pyridone-based pentamer **8a**. Other pyridone units containing different alkyl chains and the corresponding pentamers **8b**–**8f** can be made similarly.

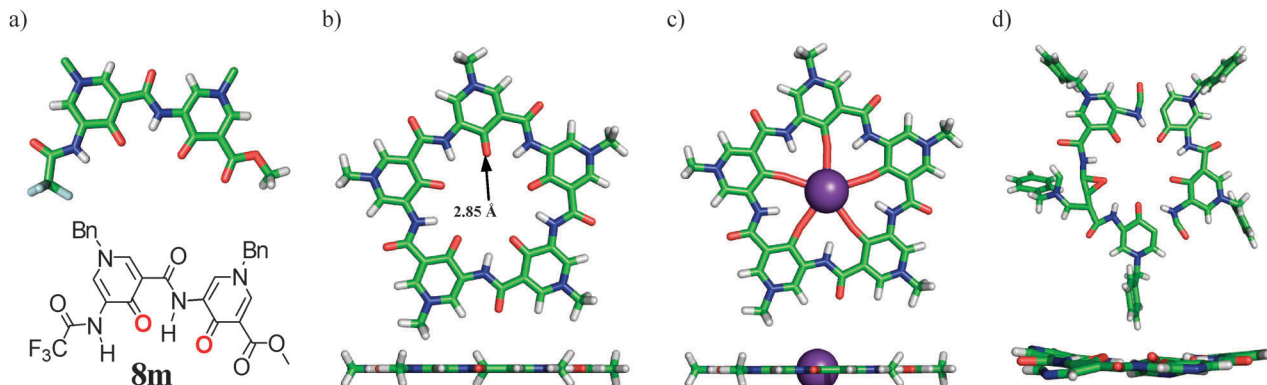


Fig. 9 (a) Chemical and crystal structures of dimer **8m**. (b) Top and side views of computationally optimized structures for pyridone-based pentamers **8a–8f** at the B3LYP/6-31G(d) level in (b) free and (c) K^+ -complexed forms, illustrating perfect *fivefold*-symmetric planarity in the pentameric backbones with and without metal ions. (d) Top and side views of a partially refined crystal structure of pentamer **8a**. A cavity radius of 2.85 Å is clearly present in the pentamer. In both (b) and (c), the exterior side chains are methyl groups.

solubility test: **8b** is sparingly soluble in DMSO at room temperature (<0.01 mM at room temperature); addition of one equivalent of Li^+ to Cs^+ tetraphenylborate (BPh_4^-) salts invariably facilitates dissolution of more than 20 mM of **8b** into DMSO. Following Cram's method of picrate extraction experiments at 10 mM of **8b** in a $\text{H}_2\text{O}-\text{CHCl}_3$ system,⁶⁶ the binding constants for complexing all the five alkali metal ions by **8b** were determined to be around 10^8 M^{-1} .²² This strong binding between **8b** and alkali metal ions is about 5 orders of magnitude higher than the equivalent 18-crown-6 under the identical conditions. Interestingly, the formed highly stable complexes can be detected using thin layer chromatography (TLC).

Further calculations on the complexes formed between the pentamer and Li^+ , Na^+ , Rb^+ and Cs^+ ions suggest that, except for Cs^+ ion (Fig. 10), the other three metal ions similarly stay coplanar with the plane of the pentameric backbone (Fig. 10a and b). This planar geometry implies a possibility of forming ion pair-mediated 1D stacked structures in the presence of monovalent anions such as Cl^- and Br^- (Fig. 10). This turns out to be the case: by slow diffusion of ethyl acetate into a DMSO or MeOH into a CHCl_3 solution, each containing 1 : 1 ratio of pentamer (**8a** or **8b**) and the respective MCl or MBr salts ($\text{M} = \text{Li}^+, \text{Na}^+, \text{K}^+, \text{Rb}^+$ and Cs^+), fibers of varying morphologies were produced. Among a total of 20 combinations examined,

only three combinations (**8a** + RbBr , **8b** + NaCl and **8b** + RbCl) do not give rise to significant fiber formation. The transmission electron microscopy images (TEM) of varying shapes of the fibers, nanorods and nanoropes produced from the other 17 combinations are representatively presented in Fig. 11a. In particular, KBr salts combine with **8b** to produce well-defined nanorods, typically measuring 50–200 nm in width and 1–3 μm in length, and **8b** in the presence of NaBr salts assembles into virtually endless nanoropes, each with a uniform diameter from 0.2 to 1 μm . These nanoropes are very flexible and easily coiled as exemplified by a single nanorope of $\sim 0.5 \mu\text{m}$ in thickness. Selective energy dispersive X-ray analyses on several of these fibers formed between **8a** and CsBPh_4 or KCl , and between **8b** and NaBr or KBr reveal the elemental occurrence of Cs, K/Cl, Na/Br and K/Br in these fibers, respectively, unambiguously confirming their incorporation into the fibers.

Additional calculations on the possible 1D structure formed from [**8a**– KBr] reveal the twist packing where vertically adjacent pentamers are alternatively twisted by 32° – 33° to be the preferred structure (Fig. 11b), and is more stable by 46.32 kcal mol^{−1} than the alternative eclipsed packing where pentamers are vertically aligned and superimposable over each other. By allowing anions to sit inside the columns and between cations, the 1D fibrillar structures should become more stable due to the

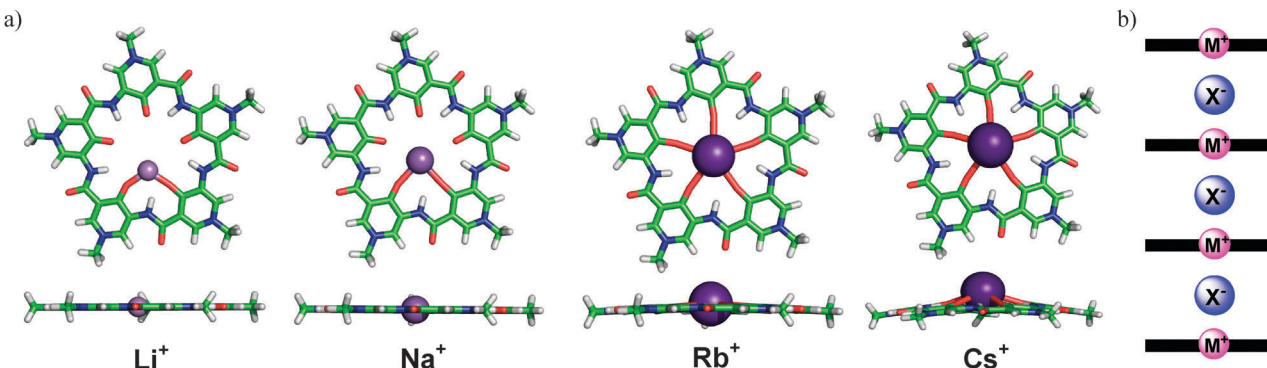


Fig. 10 (a) Computationally optimized structure of complexes formed between the pyridone pentamer and alkaline metal ions at the level of B3LYP/6-31G(d); also see Fig. 9c for the potassium complex. (b) A schematic diagram, depicting the possible formation of ion pair-mediated 1D columnar structure.

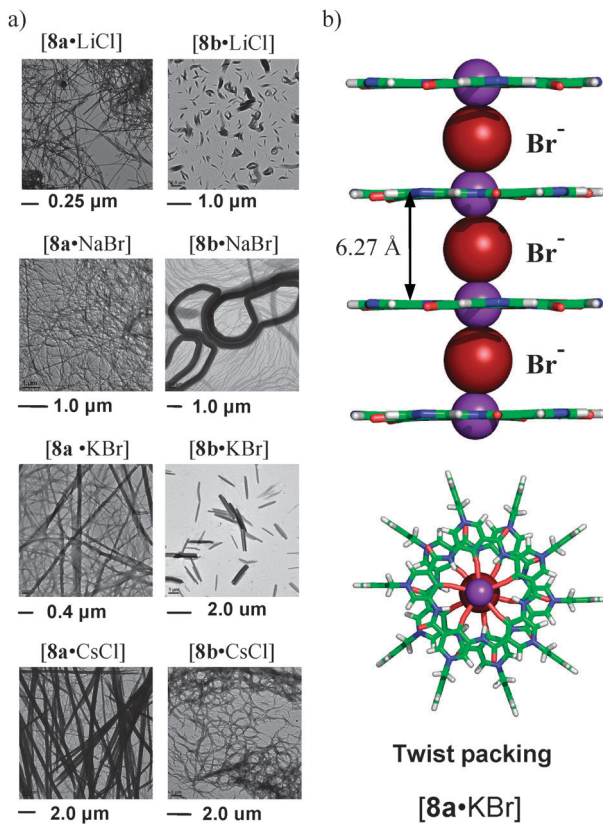


Fig. 11 (a) Selected TEM images illustrating the fibrillation induced by alkali ion pairs M^+X^- . (b) Computationally optimized structure of 1D columnar aggregates for $[8a \cdot KBr]_n$ fibers at the level of B3LYP/6-31G(d) under periodic boundary conditions. In (b), side view with their exterior side chains removed illustrates the inter-planar distances that dictate the strength of ionic interactions and the top-down view illustrates the twist packing mode. In the CPK models, $K^+ = 1.38 \text{ \AA}$ and $Br^- = 1.95 \text{ \AA}$.

existence of favorable ionic interactions and a concurrent reduction in electrostatic repulsions occurring among cations from the vertically aligned adjacent macrocycles if anions are to occupy the inter-columnar spaces. The formation of this ion pair-induced 1D columnar structure can be supported by the anion exchange experiments where fibers formed from **8a** and KCl or KBr, *i.e.*, **8a**-KCl or **8a**-KBr fibers, were suspended in MeOH solution and treated, respectively, with a large excess of

tetrabutylammonium bromide (TBABr) or TBACl. These exchange experiments show that $\sim 91\text{--}96\%$ Cl^- anions trapped in the **8a**-KCl fibers can be exchanged by excess Br^- anions, while only $\sim 26\text{--}30\%$ Br^- anions in the **8a**-KBr fibers remains exchangeable by excess Cl^- anions, suggesting anions to stay inside the column, rather than the inter-columnar spaces, and that KBr stabilizes the 1D fibrillar structures formed from **8a** better than KCl.

2.3 Fluorobenzene-based pentamers^{34,35}

Inspired by the recent works^{52,55} on the use of aromatic fluorine atoms to form intramolecular H-bonds to effectively constrain the aromatic backbones and following our methoxybenzene- and pyridone-based pentameric molecular designs (Fig. 4 and 8), aromatic fluoropentamer **9** was conceived (Fig. 12a). The *ab initio* computational molecular model at the B3LYP/6-31G(d) level reveals fascinating fivefold symmetric planarity (Fig. 12b) verifiable by its crystal structure (Fig. 12c). Our varying efforts toward elucidating the binding of metal ions by **9** demonstrate no detectable bindings between them, confirming the covalently bound fluorine atom to be a weak cation binder. This weak binding character of F-atoms is highly desired particularly with respect to a strong binding by pyridone O-atoms²² and a moderate binding by methoxy O-atoms. These cation binders with varying binding affinities are important since the modular nature of the pentameric backbones suggests a high likelihood to achieve the synthesis of hybrid pentamers such as **10** composed of exchangeable units such as methoxybenzene (**A**), hydroxybenzene (**B**), pyridone (**C**), and fluorine-containing ones (**D**) (Fig. 12d). By further combining these cation binders with the pyridine-based motifs recently developed in our lab,^{36–41} more diverse structures can be created. The ability to do so should lead to a new generation of macrocyclic receptors that feature the variable components in their main chain backbone and that are possibly endowed with the highly tunable cation-binding affinities.

Another important intention to investigate the aromatic fluoropentamer **9** is to look into whether or not and how regular pentagons of uniform size can achieve ultradense packing in the 2D plane. This is a scientifically bewildering

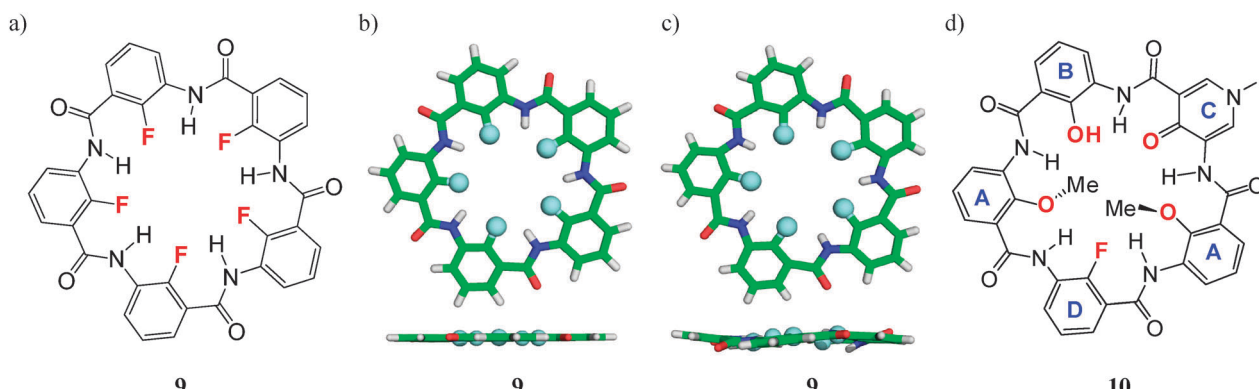


Fig. 12 (a) Structure of fluorobenzene-based pentamer **9**, top and side views of (b) computationally optimized structure of **9** at the B3LYP/6-31G(d) level and (c) its crystal structure. (d) A representative hybrid pentamer **10** composed of four different building blocks. Cyan spheres = fluorine atoms.

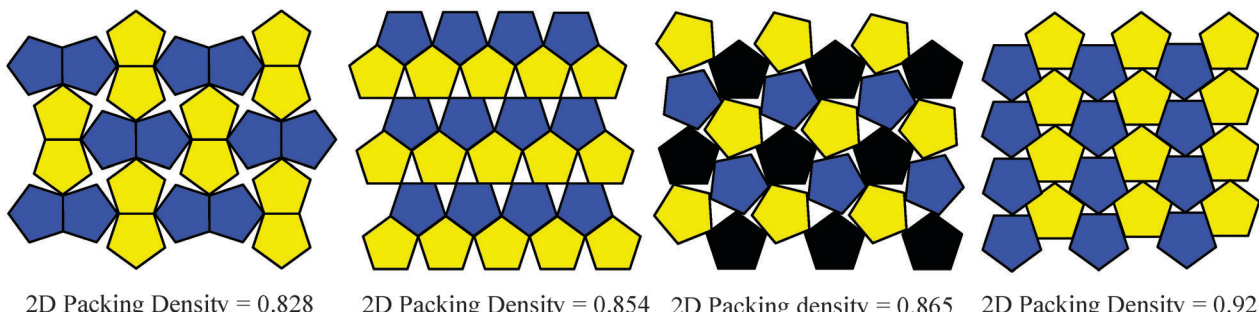


Fig. 13 Mathematically constructed periodic 2D packing patterns and packing densities by non-overlapping equal regular pentagons in the plane. The densest packing containing hexagonally arranged pentagons has a packing density of 0.921.

puzzle, for which an incorrect solution and a wrong perception is widely circulated in the literature until our report. We identified this elusive question for study in 2009 when we came across a number of references^{67–71} that all pointed to a great difficulty for regular pentagons to form a densely packed crystal lattice in a flat 2D space even though, mathematically, equal regular pentagons can form compact 2D crystal lattices (Fig. 13).^{72–76} The periodic densest packing configuration of pentagons in the plane has a 2D packing density of 0.921, and is built of alternating striped rows of pentagons pointing to opposite directions. This produces a congruent arrangement of hexagonally coordinated pentagons with *p2mg* symmetry that overcomes the symmetry mismatch between pentagons and the 2D lattice. This densest six-neighbour lattice packing was first conjectured by Henley in 1986⁷⁴ and mathematically substantiated by Kuperberg and Kuperberg in 1990.⁷⁷

A few recent attempts employed fivefold symmetric bowl-shaped corannulene and its derivatives produced either a low packing density of 0.765 for ordered 2D packing by pentagons⁷⁰ or surface-induced trimerization of pentagons with a packing intensity less than 0.725.⁷¹ We envisioned that one key to possibly solve the periodic packing problem faced by regular pentagons rests on our ability to produce fivefold symmetric, planar molecules that could resemble the overall shape of a hard pentagon. Another key is to fabricate “sticky” edges and vertices into the exterior surface of the pentagon such that these pentagons can “stick” to each other to possibly form the densest packing in the plane. With these design principles, aromatic fluoropentamer **9** was conceived and made to explore its possible shape, molecular symmetry and solid state packing. After more than six months of unsuccessful attempts, single crystals of **9** were finally obtained by slow cooling of a solution containing $\sim 1.1 \text{ mg ml}^{-1}$ of **9** in hot DMSO from 110 °C to 25 °C over three months (Fig. 12c).³⁴

Analysis of the solid state packing pattern in **9** reveals the long-awaited densest striped crystalline lattice (Fig. 14a and b) harmonically built from pure pentagon-shaped molecules that pack precisely in the manner as the mathematically verified six-neighbour densest packing should pack (Fig. 13).³⁴ Each pentamer presents five complementary ‘sticky’ edges and one vertex to attract the adjacent six neighbours by means of H-bonding specificities of three types, *i.e.*, two edge-to-vertex, two smaller edge-overlap and two larger edge-overlap bonding

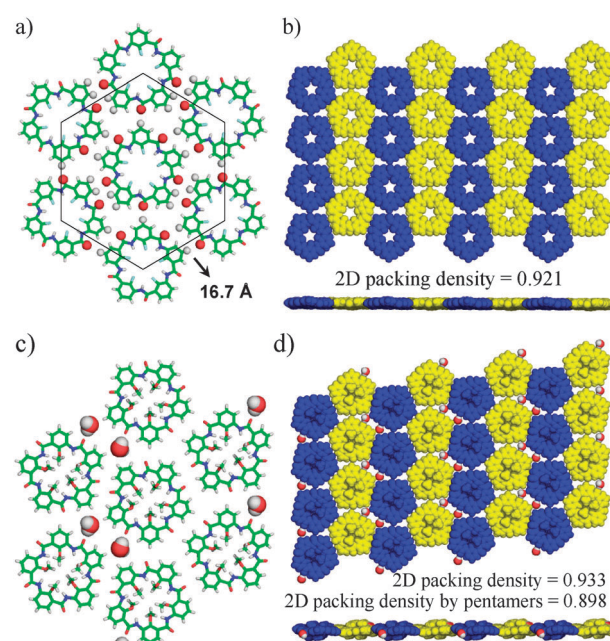


Fig. 14 Crystal structure and 2D molecular packing by macrocyclic fluoropentamer **9** and pentamer **6**. (a) Pseudo-hexagonal arrangement with a side length of 16.7 Å. Represented as small spheres are those partially charged ‘sticky’ hydrogen (gray) and oxygen (red) atoms that are involved in C=O...H-C H-bonds, allowing a tight packing of pentagon-shaped molecules. (b) Top and side views of alternating striped lattice packing in **9**, consisting of pentagons pointing to opposite directions in the CPK model, reproducing the densest mathematical crystal by pentagons (Fig. 13). (c) Distorted hexagonal unit consisting of seven water molecules and seven molecules of **6**. (d) Top and side views of the alternating striped lattice packing of **6** in the CPK model.

contacts. All these specific H-bonding interactions are mediated by weak C-H...O=C H-bonding forces. Because of these specific H-bonds conserved among pentamers that continue across the 2D lattice, minimization of the gaps among ‘sticky’ pentamers in the 2D plane is as good as the mathematically conceived packing lattice. Thus our crystal has an experimentally determined 2D packing density of 0.921, a value theoretically predicted to be the largest possible.

Re-examining the crystal structure of **6** reported by us in 2008³¹ reveals a six-neighbour packing pattern similar to **9** with long-range order and translational symmetry in the plane (Fig. 14c and d). To accommodate the water molecules in the

lattice, (i) the gaps among pentamers become larger, reducing the 2D packing density by pentamers down to 0.898 with a further contribution of a packing density of 0.035 from seven water molecules, and (ii) each pentamer makes two edge-to-vertex, one smaller and one larger edge-overlap, and one full edge contacts with its five close neighbours, leaving the sixth neighbour interacting with it through two water molecules.

By crystallizing a pentagon-shaped planar molecule **9** along with **6**, we (i) prove, for the very first time, that pentagons are compatible with the crystal lattice, and can pack highly densely and crystallographically, (ii) offer the inspiring experimental insights into the ingenious way pentagons used to naturally overcome the symmetry mismatch between pentagons and the crystal lattice, (iii) illustrate the remarkably adaptive nature of rigid pentagonal tiles in accommodating impurities such as water molecules in the packing lattice, and (iv) confirm that the mathematically sketched densest 2D packing by pentagons indeed can have an experimentally verifiable 2D packing density of as high as 0.921.

The crystal structure of **9** additionally shows that the ordered 2D lattices associate further to form a 3D layer-by-layer structure *via* a combination of aromatic $\pi\cdots\pi$ stacking interactions and numerous inter-planar H-bonds ($\text{C}=\text{O}\cdots\text{H}-\text{N} = 2.50 \text{ \AA}$, Fig. 15), resulting in a very short inter-planar distance of $\sim 3.1 \text{ \AA}$. We believed that macrocyclic analogues derived from **9** that bore suitably modified hydrocarbon chains and enhanced solubilities could be the gelators. Their gelating ability should derive firstly from their tendency to form 1D stacked fibrillar structures that are stabilized by both inter-planar H-bonds and $\pi\cdots\pi$ stacking forces, followed by the inter-columnar association *via* hydrophobic hydrocarbon chains to form a 3D gelling network, resulting in the gel by trapping organic solvents through surface tension and capillary forces. The ability of **11a** and **11b** to serve as 2D planar macrocyclic gelators was examined in a variety of

Table 2 Minimum gelation concentrations for pentamers **11a** and **11b** in different solvents at room temperature^a

Solvents	11a (mM/wt%)	11b (mM/wt%)
<i>n</i> -Hexane	2.67/0.51 (tr)	1.61/0.37 (tr)
Ethyl acetate	6.40/0.88 (op)	5.03/0.86 (op)
Diethyl ether	4.72/0.82 (op)	14.88/3.18 (op)
Cyclohexane	5.57/0.89 (tr)	S
Dioxane	5.70/0.69 (op)	20.40/3.02 (op)

^a Abbreviations: S = soluble, tr = transparent, op = opaque.

organic solvents by the “stable to inversion” method.³⁵ Table 2 lists the solvents that can gel with **11a** and **11b** at room temperature. In other solvents, **11a** and **11b** are either insoluble or too soluble (>25 mM), resulting in no gel formation. In both *n*-hexane and ethyl acetate, **11b** carrying longer aliphatic side chains functions as a better gelator than **11a** carrying shorter ones. Pentamer **11a**, however, possesses a better gelating ability than **11b** when diethyl ether, cyclohexane and dioxane are used as the solvents, probably due to the much enhanced solubility of **11b** in these solvents. The minimum gelation concentrations (MGCs) for **11a** and **11b** in *n*-hexane are as low as 2.67 mM and 1.61 mM, which correspond to 2.8×10^3 and 4.8×10^3 solvent molecules being efficiently trapped on average by just one macrocyclic gelator molecule of **11a** and **11b**, respectively.³⁵

The TEM images of these gels demonstrate the extensive formation of nanofibers, presumably resulting from inter-columnar associations of the 1D H-aggregates, for **11a** in *n*-hexane (Fig. 15c), cyclohexane (Fig. 15d) and ethyl acetate. These seemingly endless nanofibers typically measure between 100 and 250 nm in width, and structure a 3D knotted network able to “freeze” solvent molecules to form the gel. For **11b**, fiber formation is also observed in ethyl acetate (Fig. 15e) and *n*-hexane.

3. H-bonded macrocycles of varying types and their associated functions

Prior to and after our synthetic realization of H-bonded macrocyclic pentamer **6** and its other family members such as **7a**, **8a** and **9**, a number of H-bonded macrocycles of varying sizes and structures with their aromatic backbones rigidified by multiple-center H-bonding systems have been reported. On the basis of how the aromatic repeating units are linked by linkages of varying types, this section will be divided to include macrocycles containing amide and non-amide linkages.

3.1 Aryl amide macrocycles

The first example documented in the literature is the symmetrical AB-type hexameric aryl amide family of macrocycles **12** composed of symmetrical diacid and diamine building blocks by the group of Gong in 2004 (Fig. 16).²⁰ **12** encloses a non-collapsible internal cavity of $\sim 8 \text{ \AA}$ in radius that is decorated by six carbonyl O-atoms in three-fold symmetry, and is found to be able to recognize guanidinium cations highly selectively,²⁴ and to selectively extract lanthanide and thorium over alkali metal cations from aqueous solutions into dichloromethane, probably with a 1 : 1 stoichiometry.²³ Given their nearly planar

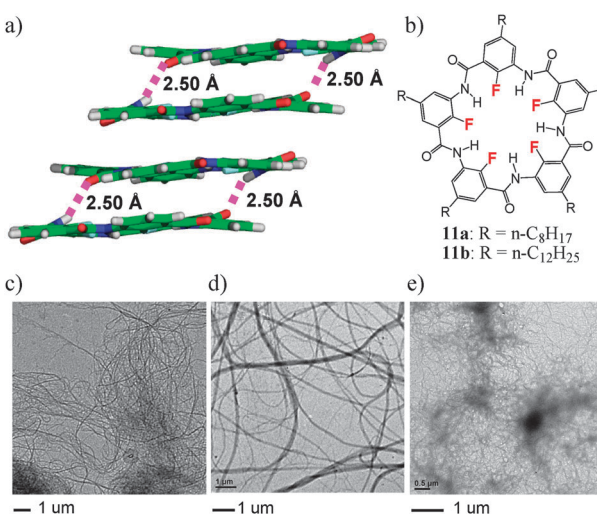


Fig. 15 (a) Formation of discrete pairs of isolated H-bonds (2.50 \AA) between every two pentamers that stabilize the inter-planar stacking as seen in the crystal structure of **9**. (b) Structures of aromatic fluoropentamers **11** containing long *n*-alkyl chains for studying their gelation properties. TEM images of the as-formed gels of **11a** in (c) *n*-hexane and (d) cyclohexane, and (e) of **3** in ethyl acetate.

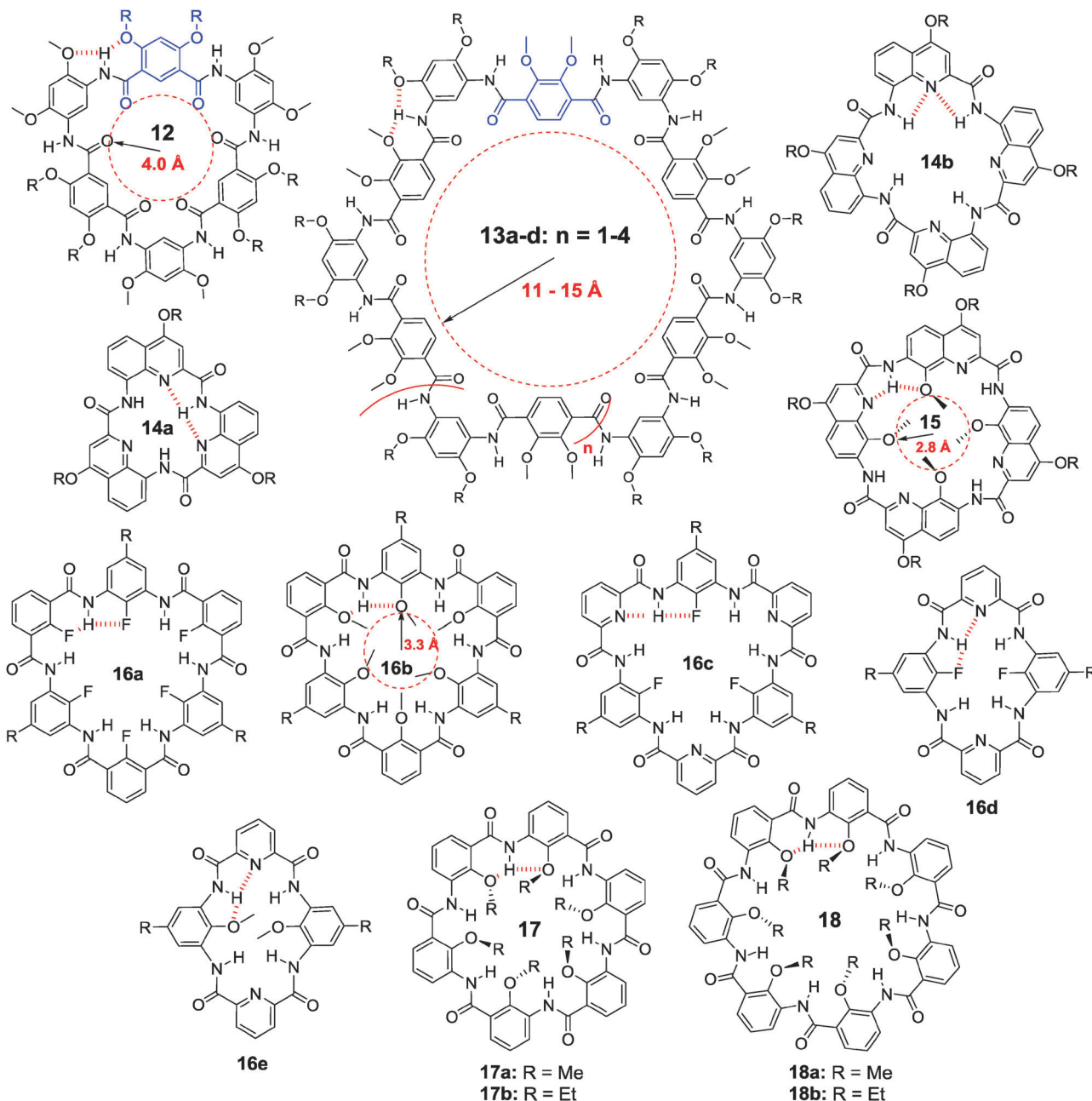


Fig. 16 Structures of shape-persistent H-bonded aryl amide macrocycles. The cavity size is measured from the cavity center to the nucleus.

geometry, cavity-containing macrocycles **12** can assemble into 1D columnar aggregates that are stable in the lipid bilayers and function as transmembrane channels with very large conductances of sodium ions (Fig. 17).²⁵ The most active derivative of **12** shows an ion exchange rate constant of $5.65 \pm 1.62 \text{ s}^{-1}$, a value that is about half of that of channel-forming gramicidin but over an order of magnitude higher than valinomycin that serves as an ion carrier. Gong and co-workers further showed that the curvature of cyclic backbones can be dramatically tuned by replacing the *meta*-linked dicarboxylic acid groups in **12** with the *para*-linked one as in **13**.⁷⁸ This replacement leads to very large 14- to 18-residue macrocycles **13** containing an interior cavity of up to 15 Å in radius.

Huc and co-workers reported the synthesis of cyclic trimer **14a** and highly strained cyclic tetramer **14b**, both of which are derived from the 8-amino-2-quinolinecarboxylic acid motif.²⁷ In this case the cyclic trimer forms as anticipated and is quite planar as shown by its crystal structure. It is therefore of interest to note that the highly strained cyclic tetramer **14b** can be produced in 20% yield. The X-ray crystal structure of **14b** confirms a strong deviation of its macrocyclic backbone from planarity, leading to a saddle shape (Fig. 18a). This saddle shape results in a loss of two intramolecular H-bonds in the inner rim, and breaks two pairs of conjugations between the aryl and their adjacent amide groups as the dihedral angle between them was found to be near 90°. This saddle shape

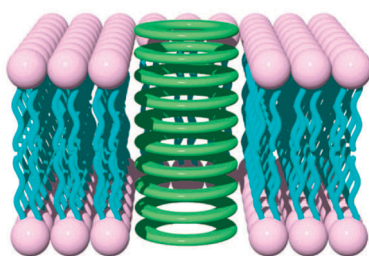


Fig. 17 Macrocycles **12** can assemble into a channel structure in the hydrophobic environment of a lipid bilayer and are able to transport sodium ions with a rate constant of as fast as $5.65 \pm 1.62 \text{ s}^{-1}$. Reprinted from *J. Am. Chem. Soc.*, 2008, **130**, 15784, with permission from American Chemical Society.

however gives rise to two sizable cavities between two pairs of quinoline rings facing each other, allowing **14b** to bind up to two aromatic guest molecules such as *p*-toluenesulfonic acid with a moderate association constant of $\sim 10^3 \text{ M}^{-1}$. Significantly, **14a** with amine-containing side chains was shown to strongly stabilize G-quadruplex structures of different types.²⁸ At $1 \mu\text{M}$, **14a** increases the melting points of the human telomeric G-quadruplex (h-telo) and one of the c-kit promoter G-quadruplex (c-kit) by 33.8°C and 21.4°C , respectively. By contrast, no stabilization of the duplex DNA was observed by **14a**.

It was observed in the crystal structure of a helically folded tetramer derived from the ϵ -aminoquinolinecarboxylic acid unit that the two helical ends are placed in close proximity, suggesting that approximately four units are required to form a helical turn and its intramolecular cyclization into a macrocyclic planar structure is highly possible.⁵² Along this line, Jiang and co-workers demonstrated this possibility by using the ϵ -aminoquinoline-carboxylic acid motif as the macrocyclic repeating unit to construct another new class of cyclic tetramers **15**.⁷⁹ The crystal structure shows a nearly planar H-bonded macrocyclic backbone with H-bonds of N-H \cdots O or N measuring at 2.070 – 2.211 \AA (Fig. 18b). The four interior methoxy methyl groups point up and down alternatively around the ring, and block the oxygen-containing cavity of $\sim 2.8 \text{ \AA}$ in radius. It is highly possible that the cavity may be able to bind smaller cations such as Na^+ and K^+ if the interior methyl groups

can be replaced by hydroxyl groups, followed by deprotonating hydroxyl groups to produce phenolate anions.²¹

Li and co-workers assessed the abilities of H-bonding motifs of F \cdots H-N, MeO \cdots H-N and N \cdots H-N to direct the formation of macrocyclic structures.²⁶ Depending on the types of monomer units used, 4- and 6-residue macrocycles **16a**–**16e**, containing inwardly located F, O and N-atoms that lead to intramolecular H-bonding networks for backbone rigidification, can be prepared (Fig. 16) along with a two-residue macrocycle that should be very strained. In the crystal structure of **16b**, no columnar stackings among macrocycles were observed,³⁰ and the four adjacent methyl groups unusually point to the same side of the backbone, while the remaining two point to the opposite side (Fig. 18c). This is due to the more favored π - π stacking involving one diamidobenzene unit from one molecule of **16b** and another identical unit from the neighbouring molecule. In **16e**, the two interior methyl groups point to different sides of the cyclic backbone with the two benzene rings deviating slightly from the plane. Interestingly, both **16a** and **16b** display good binding affinities toward C_{60} and C_{70} . By using fluorescence titration experiments, the association constants of complexes **16a**· C_{60} , **16a**· C_{70} , **16b**· C_{60} and **16b**· C_{70} in chloroform were determined to be $5.9 \times 10^4 \text{ M}^{-1}$, $9.1 \times 10^4 \text{ M}^{-1}$, $2.5 \times 10^4 \text{ M}^{-1}$ and $4.1 \times 10^4 \text{ M}^{-1}$, respectively. It was proposed that macrocycles might interact with an extended equatorial region of C_{70} via the stacking and that complex **16a**· C_{60} is formed as a result of a combination of the extended fluoroarene- π ²⁴ and solvophobic interactions (Fig. 18d).

As demonstrated by the crystal structure of pentamer **6** (Fig. 5), the planar pentameric backbone is preferred by methoxybenzene-based units. Computationally, pentamer **6** is also the most stable, and more stable than the corresponding highly strained tetramer, strained hexamer **17a** and highly strained heptamer **18a** by 4.56 , 0.52 and $1.00 \text{ kcal mol}^{-1}$ per repeating unit in acetonitrile at the B3LYP/6-31G(d) level (Fig. 19a–d). However, when the interior methoxy groups are replaced by ethoxy groups, hexamer **17b** becomes the most stable, and more stable than the corresponding tetramer, pentamer and heptamer **18b** by 4.78 , 1.03 and $4.46 \text{ kcal mol}^{-1}$

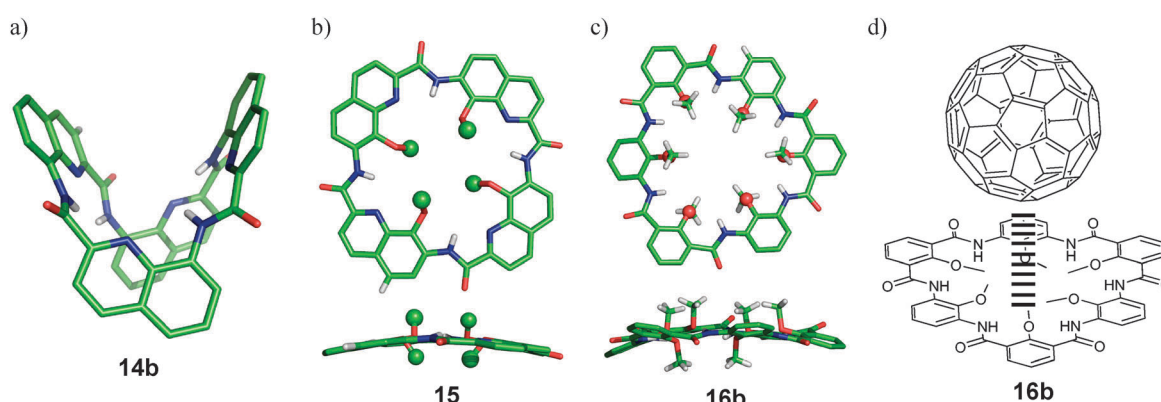


Fig. 18 (a) Side view of the crystal structure of the saddle-shaped **14b**, (b) top and side views of the crystal structure of the nearly planar **15**, enclosing a cavity of $\sim 2.8 \text{ \AA}$ in radius that is blocked by the interior methyl groups; the accurate positions of the interior methyl protons cannot be crystallographically located, (c) top and side views of the crystal structure of **16b** containing a cavity of $\sim 3.3 \text{ \AA}$ in radius is blocked by the interior methyl groups and (d) a possible interacting mode between **16b** and C_{60} . Exterior side chains and aromatic protons were removed from all the crystal structures.

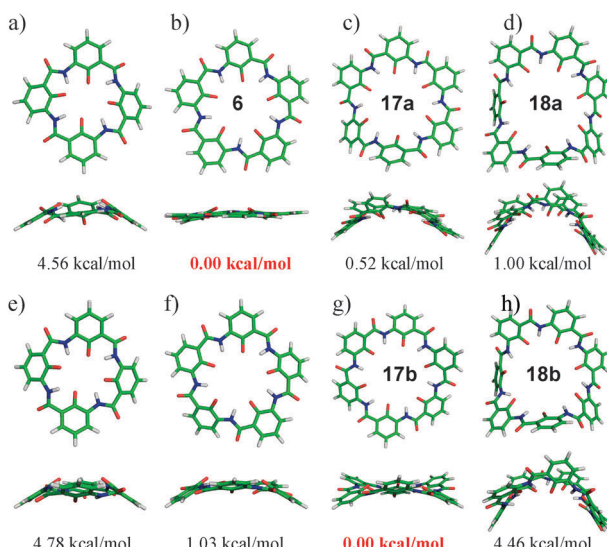


Fig. 19 Top and side views of *ab initio*-optimized structures of methoxy-containing circularly folded (a) tetramer, (b) pentamer **6**, (c) hexamer **17a** and (d) heptamer **18a** as well as ethoxy-containing circularly folded (e) tetramer, (f) pentamer, (g) hexamer **17b** and (h) heptamer **18b** in acetonitrile at the B3LYP/6-31G(d) level. The computationally derived relative energy per repeating unit among these circular foldamers is normalized based on the most stable pentamer **6** or hexamer **17b**. For clarity of the view, all the interior methyl or ethyl groups were removed.

per repeating unit (Fig. 19e–h). By fine-tuning the reaction conditions both strained hexamers **17** and heptamers **18** can be made with yields of 20–33% and 14–16%, respectively.⁸⁰

3.2 Macrocycles containing non-amide linkages

In their very recent work, MacLachlan and co-workers reported *five-fold* symmetric macrocyclic pentamers **19** (Fig. 20) with good planarity in high yields of 70–99%.⁴² The backbone is rigidified by a continuous intramolecular H-bonding network involving the hydroxyl and imine groups. On the basis of IR and ¹H NMR data, **19** probably has a structure intermediate between the enol-imine and keto-enamine tautomers, each containing a strong 3-center hydrogen bond (Fig. 21a). *Ab initio* calculations at the B3LYP/6-31G(d) level reveal a planar geometry and an interior cavity of 2.8 Å in radius for **19** in either enol-imine or keto-enamine forms (Fig. 21b and c). The enol-imine tautomer is calculated to be 4.02 kcal mol⁻¹ more stable than the keto-enamine form in the gas phase.

Gong and co-workers devised another strategy to facilitate the control of the macrocyclic cavity size.⁸¹ In this study, hydrazine linkages were introduced into the cyclic AB-type macrocycles, containing pyridine- and 2,3-dimethoxyterephthalic acid-based building blocks, respectively, to produce **20a** and **20b** with a respective cavity size of ~1 nm and >2 nm (Fig. 22a and b). Computational analyses at the level of B3LYP/6-31G(d) show that both macrocycles **20a** and **20b** adopt a planar geometry. Very recently, tetrameric macrocycles **21a**⁸² and **21b**⁸³ containing urea groups as the focal point for forming intramolecular H-bonds were also reported by the same group.

Using naphthyridine-based building blocks, Cuccia and co-workers synthesized macrocycles containing urea- (**22a**)

and formamidine-linkages (**22b**).⁷ The presence of the H-bonding network and good planarity of the synthesized macrocycle **22b** was supported by the crystal structure (Fig. 22c). And the interiorly arrayed protons involved in intramolecular H-bonds can be readily differentiated from the exterior ones on the basis of (i) hydrogen–deuterium exchange experiments, demonstrating that the interior protons being “locked” into an intramolecular H-bonding network took much longer (>30 min) to exchange with deuterons while exterior protons were completely exchanged within 5 min and (ii) variable-temperature ¹H NMR studies, illustrating a temperature-dependent chemical shift for exterior protons while the chemical shifts of the interior ones did not show a temperature-dependent behavior.

4. Rapid synthesis of H-bonded macrocycles

Efficient construction of macrocyclic backbones to derive the “macrocyclic effect” has been a constant challenge. To promote the effective macrocyclization, one-step cyclization, templated cyclization, intramolecular ring closure, intermolecular coupling, dynamic covalent bond formation and conformation-assisted macrocyclization have been developed.¹⁹ Despite these intensive efforts and synthetic advancements, most of the cyclization reactions are still carried out under conditions of high dilution, and critical challenges remain in the efficient construction of functional macrocycles.

A recent breakthrough in macrocycle synthesis was reported by Gong and co-workers in 2004.²⁰ In their report, localized three-center intramolecular H-bonding systems are utilized to efficiently preorganize the *in situ* generated intermediate acyclic hexameric oligomer into a curved conformation, bringing the reactive sites at its two ends into close proximity and readily forming the H-bonded macrocycles **12** in high isolated yields of 69–82% by coupling different diacid chlorides (**24a**) with 4,6-dimethoxy-1,3-phenylenediamine (**24b**) at a high concentration of 130 mM *via* one-pot H-bonding-directed macrocyclization reactions in about one day under very mild conditions (Fig. 23a and entry 1, Table 3). In the absence of the H-bonding networks, the yield obtained for the respective cyclic hexamers was found to be low even when the reaction was carried out in the presence of a template or under high dilution conditions as a result of the flexible backbone in the conformationally ill-defined intermediate oligomers.⁸⁴ This concept involving the use of H-bonds to direct macrocycle synthesis can be traced back to as early as 1994 when Hunter and co-workers used the pyridine carboxamides to partially rigidify the macrocyclic precursors and intermediates to be formed, producing macrocycle **23** and its other analogues with high yields of 80–90% (Fig. 23b).⁸⁵ A detailed mechanistic investigation of the H-bonding-assisted one-pot macrocyclization reaction shows that the macrocyclization is bimolecular in nature and largely kinetically controlled with the formation of larger macrocycles discouraged by the remote steric effect.⁷⁸ The suggested mechanism was further supported by the efficient synthesis of a 16-residue macrocycle **13c** in 81% yield with concurrent production of 14- and 18-residue macrocycles **13b** and **13d** (entry 2, Table 3). Although a

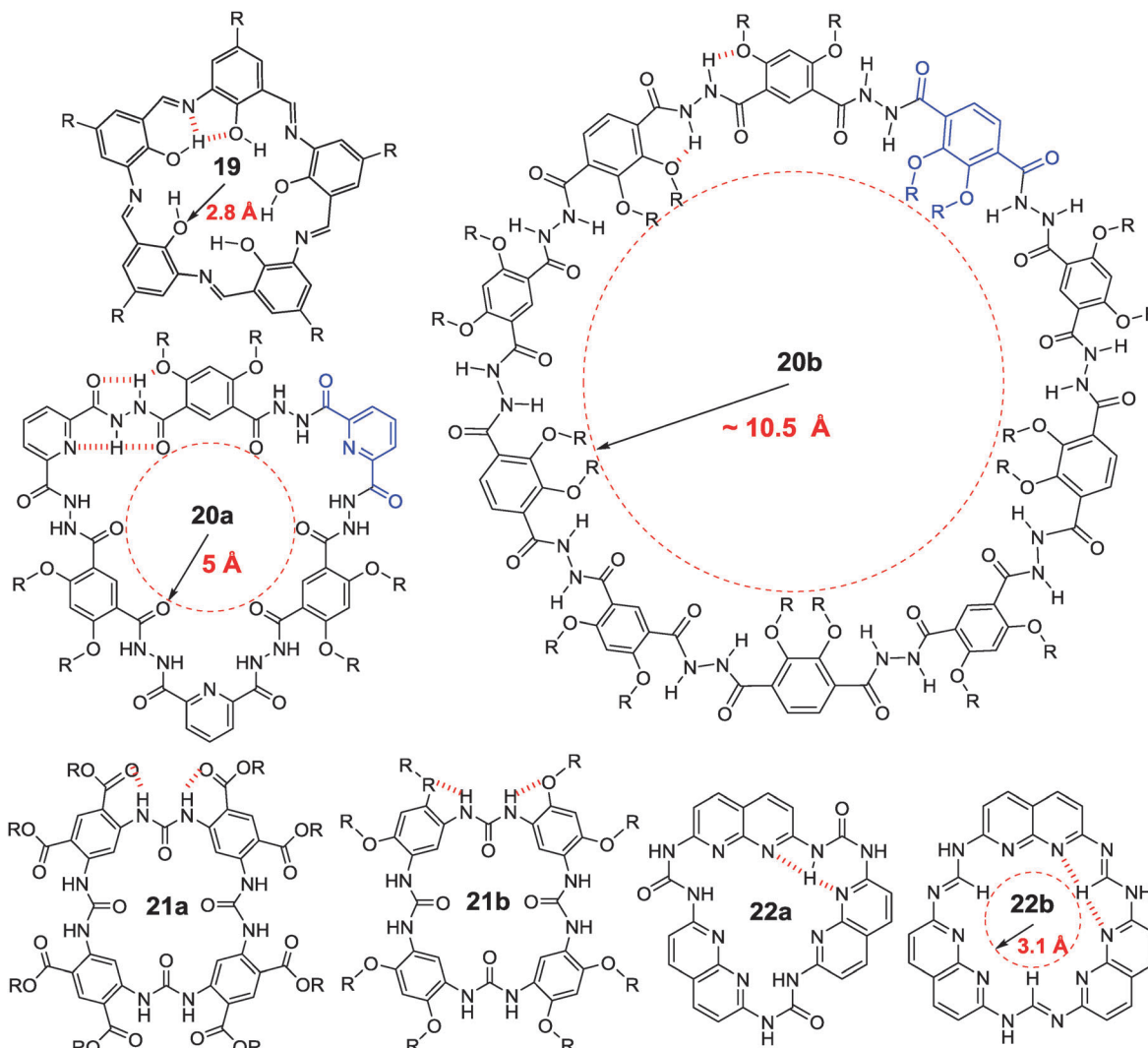


Fig. 20 Structures of macrocycles comprising Schiff-base, hydrazide, urea, and formamidine functional groups as the linkages.

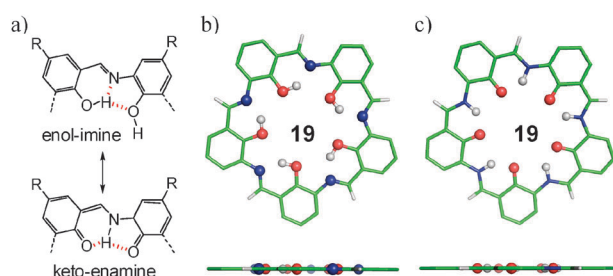


Fig. 21 (a) Tautomerization between enol-imine and keto-enamine form in **19**, each containing a 3-center H-bond that leads to the backbone rigidification. Top and side views of computationally determined structures for **19** as (b) enol-imine and (c) keto-enamine tautomers.

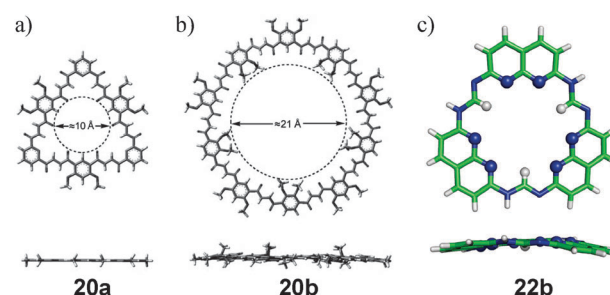


Fig. 22 Top and side views of the computationally determined structures of (a) **20a** and (b) **20b** at the level of B3LYP/6-31G(d) as well as (c) the crystal structure of **22b** containing a cavity of 3.1 Å in radius. The images in (a) and (b) were reprinted from *Angew. Chem., Int. Ed.*, 2009, **48**, 3150, with permission from John Wiley & Sons, Inc.

computational analysis suggests **13c** to be the most stable among macrocycles **13a–13d**, by alternatively performing the condensation reaction using both a monomer and a trimer as the starting oligomers, **13d** can be selectively produced in yield of 85%.

Since the work by Gong, the groups of Huc, Jiang and Li also reported the H-bonding-assisted macrocyclization of varying types, allowing macrocycles **14–16** to be prepared in high yields (entries 3–5, Table 3). The one-pot H-bonding-directed

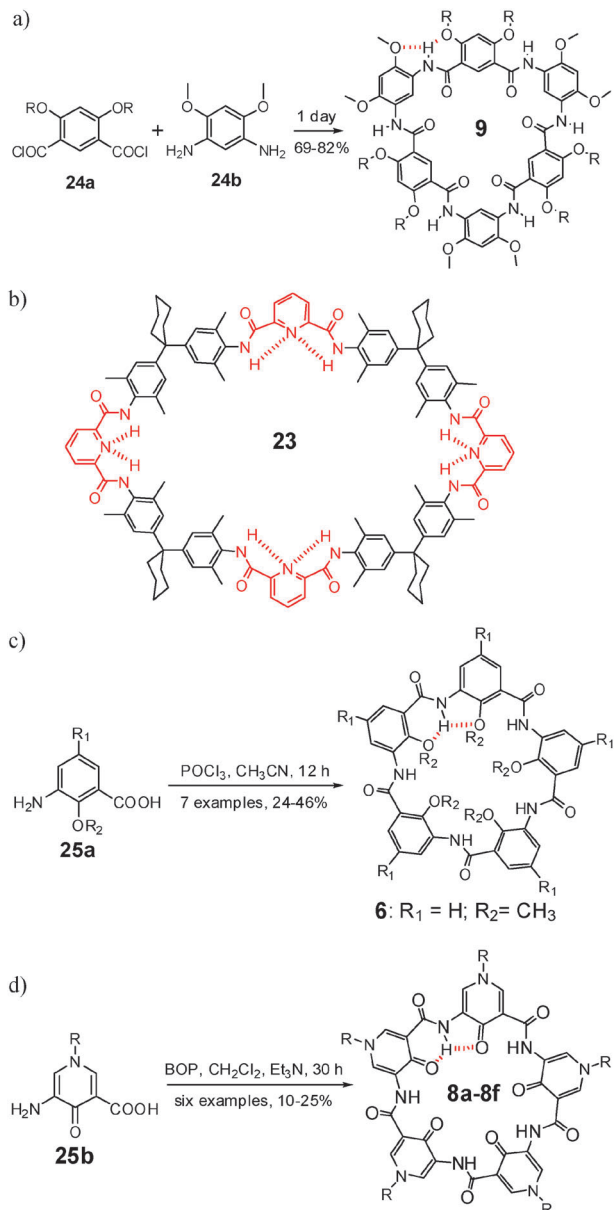


Fig. 23 (a) Synthesis of **9** by H-bonding-assisted one-pot macrocyclization, (b) one of the early macrocycles, **23**, made by Hunter *et al.* by using the H-bonds for backbone rigidification as well as one-pot synthesis of (c) **6** and its other analogues bearing different exterior and interior side chains and (d) macrocyclic pyridone pentamers **8a–8f** with precise control over the ring sizes and the variable functionalization around the periphery.

macrocyclization reactions also work with macrocycles **19–22** containing Schiff-base,⁴² hydrazide,⁸¹ urea,^{7,82,83} and formamidine⁷ linkages in good yields (entries 6–11, Table 3) as reported by the groups of MacLachlan,⁴² Gong^{81–83} and Cuccia.⁷

Considering that the macrocyclic pentamer **6** and its other family members such as **8a** and **9** were all made by the stepwise procedures with very low overall yields of ~1–5% after months' efforts, it is therefore of high interest to see if these H-bonded organic pentagons can be made by a more cost efficient and less time-consuming method or not *via* one-pot macrocyclization reactions. After testing many coupling reagents and different conditions, phosphoryl trichloride, POCl₃ was

identified as a powerful macrocyclization reagent, enabling monomeric amino acid building blocks **25a** to react to form pentamer **6** and its other analogues as the major product with yields of 24–46% at 100 mM at room temperature in HPLC grade acetonitrile (CH₃CN) containing ≤0.01% water (Fig. 23c).³² Under these conditions, ~6% of hexamer **17a** and trace amounts of heptamer **17b** were also produced, an observation that is in line with their computationally determined relative order in stability (Fig. 19).⁸⁰ By re-investigating the POCl₃-mediated one-pot reactions using dry CH₃CN, the overall yield of all 5-, 6- and 7-residue macrocycles increased from 52% (46% pentamer **6** + 6% hexamer **17a**) in "ordinary" CH₃CN to 78% in "dry" CH₃CN (40% pentamer **6** + 24% hexamer **17a** + 14% heptamer **17b**) at room temperature,⁸⁰ suggesting that even trace amounts of water present in the reaction significantly impede the one-pot macrocyclization reaction possibly by inactivating the acid chloride of intermediate oligomers. We have also reported one-pot macrocyclization reactions mediated by BOP,³³ a peptide coupling reagent that allows for pyridone-based building blocks **25b** to form cyclic planar pentamers **8a–8e** with an interior cavity of ~2.8 Å in radius that is decorated by five convergently aligned carbonyl O-atoms for efficient cation recognitions (Fig. 23d).²²

Mechanistic studies by kinetic simulations of experimental data suggested the POCl₃-mediated pentamerization to take place through a chain growth mechanism where the addition of monomer into the growing backbones is faster than other competing bimolecular reactions between two monomers or two higher oligomers (Fig. 24)⁸⁶ while the corresponding macrocyclization reactions producing strained hexamer **17** and highly strained heptamers **18** likely proceed in a bimolecular fashion involving two higher oligomers.⁸⁰ Consistent with the proposed chain-growth mechanism, our continued exploration demonstrated that POCl₃ can selectively produce hybrid macrocyclic pentamers consisting of mixed building blocks that bear different exterior side chains (Fig. 25).⁸⁷ This discovery, for the very first time, enables a regiospecific functionalization around the pentameric periphery *via* one-pot co-macrocyclization of variable repeating units.

Based on the reactivities of the newly discovered macrocyclization reagents POCl₃ and BOP, we proposed that every type of asymmetric monomer building block destined to form the most stable circularly folded oligomers may require its own unique "cognate" macrocyclization regents that ought to be "orthogonal" to each other and function well only against their own specific set of "cognate" monomer units.³³ It therefore remains as an outstanding interest to see whether the "cognate" macrocyclization regents for fluorobenzene^{34,35} and pyridine^{36–41} motifs can be identified or not to yield the circular fluoropentamer and pyridine tetramer respectively.

Very recently, we found that tetrabutylammonium chloride or bromide salts (TBACl/Br)^{85,86} are able to achieve efficient folding-promoted chemo- and regio-selective demethylations,^{88,89} eliminating up to two out of five methyl groups situated in similar macrocyclic chemical microenvironments as in **6**. By combining with the one-pot synthesis of **6** in 46% yield, macrocyclic anionic pentamers such as **7c²⁻** can now be prepared in just two steps with

Table 3 One-pot synthesis of H-bonded macrocycles from their monomeric units via H-bonding-assisted macrocyclization

Entry	Macrocyclic product	Macrocyclization conditions	Yields (%)	Ref.
1	12	Et ₃ N (2.2 equiv.), CH ₂ Cl ₂ , -20 °C, 24 h	69–82	20
2	13	Et ₃ N (3.0 equiv.), CH ₂ Cl ₂ , -30 °C for 4 h, rt for 10 h and refluxed for 2 h	>80	78
3	14	Conc. LiCl (1 M) in NMP, triphenylphosphite, 3 h	20–50	5, 27
4	15	Triphenylphosphite, THF, 65 °C	46–53	79
5	16	Et ₃ N (4.7 equiv.), THF, rt, 1 h	10–45	26
6	19	Sodium dithionite, EtOH–water, reflux for 2–4 h	70–99 ^a	
7	20	DMAP, CH ₂ Cl ₂ , 0 °C for mixing, then warmed up to rt, followed by refluxing for 24 h	72–97	81
8	21a	Triphosgene, DMAP, toluene	65–68	82
9	21b	Triphosgene, Et ₃ N, CH ₂ Cl ₂ , -75 °C for 2 h, then 5 h at rt	81	83
10	22a	1,1-Carbonyldimidazole, DMSO, 30 min under nitrogen at rt, and 120 °C under nitrogen for 24 h	64	7
11	22b	Triethyl orthoformate, DMSO, 120 °C under nitrogen for 2 h	75	7

^a An alternative route using a cyclic aminal to protect formyl groups and Pd/C for reduction of the nitro group produces the same macrocycles in refluxing ethanol in near quantitative yields. Et₃N = triethylamine; NMP = N-methyl-2-pyrrolidone; DMAP = 4-dimethylaminopyridine.

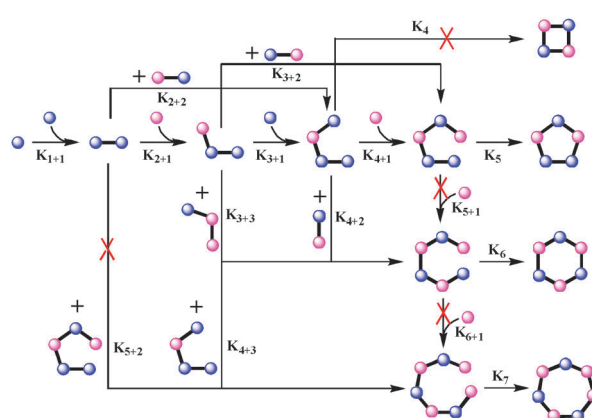


Fig. 24 Possible reaction pathways accounting for the preferred formation of acyclic oligomeric intermediates and circular pentamer **6** and its other analogues. The circular tetramers (under-shooting products) are not formed while hexamers and pentamers (over-shooting products) may be possibly formed via different pathways from the reaction. K is the reaction rate constant and $K_{n+m} = K_{m+n}$. Reactions of K_4 , K_{5+1} , K_{5+2} and K_{6+1} types are not likely based on the kinetic simulations of experimental data.

functions. Many of these macrocycles can now be rapidly prepared *via* one-pot H-bonding-directed macrocyclization with minimized side products, greatly facilitating their subsequent applications in the construction of functional supramolecular architectures and materials. As illustrated by hybrid pentamer **10** (Fig. 12d), our macrocyclic pentameric system is characterized by a small cavity size of $\sim 2.8 \text{ \AA}$ in radius suitable for cation recognition, and further by their cyclic backbones modularly tunable by using building blocks A, B, C or D in different ratios and at different positions (Fig. 12d). These notable traits enable a combinatorial production of an enriched family of modularly engineerable cavity-forming macrocyclic pentamers. Their shape-consistent skeletons effectively preorganize electronic (*e.g.*, oxygens and fluorines) and steric/hydrophobic (*e.g.*, methyl groups and hydrogens) features into a convergent alignment that may eventually allow the circular pentamers to tightly, yet selectively, bind metal cations. Accordingly, diverse and influential functions crossing traditional boundaries are likely to arise from the existing and quickly emerging macrocycles of varied designs and structures.

Acknowledgements

Financial support for the works described in this review article to H.Z. by National Research Foundation Competitive Research Programme Grant (R-154-000-529-281), NUS AcRF Tier 1 grant (R-143-000-506-112) and SPORE (COY-15-EWI-RCFSA/N197-1) is greatly acknowledged.

Notes and references



Fig. 25 POCl₃-mediated regiospecific functionalization around the pentamic periphery can be achieved by reacting monomers (purple circles) with higher oligomers (blue circles) that bear different exterior side chains.

an overall yield of $\sim 45\%$ within a day rather than $\sim 5\%$ yields after months' efforts. This is important given their recently demonstrated abilities to differentiate between Na⁺/K⁺ and Rb⁺/Cs⁺ ions in a highly selective and tight fashion.²²

5. Conclusions

As summarized here, a number of H-bonded macrocycles have recently appeared in the literature along with their varied

- J. L. Sessler and D. Seidel, *Angew. Chem., Int. Ed.*, 2003, **42**, 5134–5175.
- R. Misra and T. K. Chandrashekhar, *Acc. Chem. Res.*, 2008, **41**, 265–279.
- W. Zhang and J. S. Moore, *Angew. Chem., Int. Ed.*, 2006, **45**, 4416–4439.
- S. Brooker, *Coord. Chem. Rev.*, 2001, **222**, 33–56.
- N. E. Borisova, M. D. Reshetova and Y. A. Ustynyuk, *Chem. Rev.*, 2007, **107**, 46–79.
- J. Blankenstein and J. P. Zhu, *Eur. J. Org. Chem.*, 2005, 1949–1964.
- L. Y. Xing, U. Ziener, T. C. Sutherland and L. A. Cuccia, *Chem. Commun.*, 2005, 5751–5753.
- J. M. Holub, H. J. Jang and K. Kirshenbaum, *Org. Lett.*, 2007, **9**, 3275–3278.
- F. Campbell, J. Plante, C. Carruthers, M. J. Hardie, T. J. Prior and A. J. Wilson, *Chem. Commun.*, 2007, 2240–2242.

- 10 A. Yokoyama, T. Maruyama, K. Tagami, H. Masu, K. Katagiri, I. Azumaya and T. Yokozawa, *Org. Lett.*, 2008, **10**, 3207–3210.
- 11 L. He, Y. An, L. H. Yuan, W. Feng, M. F. Li, D. C. Zhang, K. Yamato, C. Zheng, X. C. Zeng and B. Gong, *Proc. Natl. Acad. Sci. U. S. A.*, 2006, **103**, 10850–10855.
- 12 M. Geng, D. Zhang, X. Wu, L. He and B. Gong, *Org. Lett.*, 2009, **11**, 923–926.
- 13 S. H. Gellman, *Acc. Chem. Res.*, 1998, **31**, 173–180.
- 14 D. J. Hill, M. J. Mio, R. B. Prince, T. S. Hughes and J. S. Moore, *Chem. Rev.*, 2001, **101**, 3893–4011.
- 15 B. Gong, *Acc. Chem. Res.*, 2008, **41**, 1376–1386.
- 16 I. Saraogi and A. D. Hamilton, *Chem. Soc. Rev.*, 2009, **38**, 1726–1743.
- 17 G. Guichard and I. Huc, *Chem. Commun.*, 2011, **47**, 5933–5941.
- 18 D.-W. Zhang, X. Zhao, J.-L. Hou and Z.-T. Li, *Chem. Rev.*, 2012, **112**, 5271–5316.
- 19 W. Q. Ong and H. Q. Zeng, *J. Inclusion Phenom. Macrocyclic Chem.*, 2012, DOI: 10.1007/s10847-10012-10243-10844.
- 20 L.-H. Yuan, W. Feng, K. Yamato, A. R. Sanford, D. Xu, H. Guo and B. Gong, *J. Am. Chem. Soc.*, 2004, **126**, 11120–11121.
- 21 B. Qin, C. L. Ren, R. J. Ye, C. Sun, K. Chiad, X. Y. Chen, Z. Li, F. Xue, H. B. Su, G. A. Chass and H. Q. Zeng, *J. Am. Chem. Soc.*, 2010, **132**, 9564–9566.
- 22 C. L. Ren, V. Maurizot, H. Q. Zhao, J. Shen, F. Zhou, W. Q. Ong, Z. Y. Du, K. Zhang, H. B. Su and H. Q. Zeng, *J. Am. Chem. Soc.*, 2011, **133**, 13930–13933.
- 23 L. J. Zhong, L. Chen, W. Feng, S. L. Zou, Y. Y. Yang, N. Liu and L. H. Yuan, *J. Inclusion Phenom. Macrocyclic Chem.*, 2012, **72**, 367–373.
- 24 A. R. Sanford, L. H. Yuan, W. Feng, K. Y. R. A. Flowers and B. Gong, *Chem. Commun.*, 2005, 4720–4722.
- 25 A. J. Helsel, A. L. Brown, K. Yamato, W. Feng, L. H. Yuan, A. J. Clements, S. V. Harding, G. Szabo, Z. F. Shao and B. Gong, *J. Am. Chem. Soc.*, 2008, **130**, 15784–15785.
- 26 Y. Y. Zhu, C. Li, G. Y. Li, X. K. Jiang and Z. T. Li, *J. Org. Chem.*, 2008, **73**, 1745–1751.
- 27 H. Jiang, J.-M. Léger, P. Guionneau and I. Huc, *Org. Lett.*, 2004, **6**, 2985–2988.
- 28 P. S. Shirude, E. R. Gillies, S. Ladame, F. Godde, K. Shin-Ya, I. Huc and S. Balasubramanian, *J. Am. Chem. Soc.*, 2007, **129**, 11890–11891.
- 29 Y. Yan, B. Qin, Y. Y. Shu, X. Y. Chen, Y. K. Yip, D. W. Zhang, H. B. Su and H. Q. Zeng, *Org. Lett.*, 2009, **11**, 1201–1204.
- 30 Y. Yan, B. Qin, C. L. Ren, X. Y. Chen, Y. K. Yip, R. J. Ye, D. W. Zhang, H. B. Su and H. Q. Zeng, *J. Am. Chem. Soc.*, 2010, **132**, 5869–5879.
- 31 B. Qin, X. Y. Chen, X. Fang, Y. Y. Shu, Y. K. Yip, Y. Yan, S. Y. Pan, W. Q. Ong, C. L. Ren, H. B. Su and H. Q. Zeng, *Org. Lett.*, 2008, **10**, 5127–5130.
- 32 B. Qin, W. Q. Ong, R. J. Ye, Z. Y. Du, X. Y. Chen, Y. Yan, K. Zhang, H. B. Su and H. Q. Zeng, *Chem. Commun.*, 2011, **47**, 5419–5421.
- 33 Z. Y. Du, C. L. Ren, R. J. Ye, J. Shen, Y. J. Lu, J. Wang and H. Q. Zeng, *Chem. Commun.*, 2011, **47**, 12488–12490.
- 34 C. L. Ren, F. Zhou, B. Qin, R. J. Ye, S. Shen, H. B. Su and H. Q. Zeng, *Angew. Chem., Int. Ed.*, 2011, **50**, 10612–10615.
- 35 C. L. Ren, S. Y. Xu, J. Xu, H. Y. Chen and H. Q. Zeng, *Org. Lett.*, 2011, **13**, 3840–3843.
- 36 W. Q. Ong, H. Q. Zhao, Z. Y. Du, J. Z. Y. Yeh, C. L. Ren, L. Z. W. Tan, K. Zhang and H. Q. Zeng, *Chem. Commun.*, 2011, **47**, 6416–6418.
- 37 W. Q. Ong, H. Q. Zhao, X. Fang, S. Woen, F. Zhou, W. L. Yap, H. B. Su, S. F. Y. Li and H. Q. Zeng, *Org. Lett.*, 2011, **13**, 3194–3197.
- 38 H. Q. Zhao, W. Q. Ong, F. Zhou, X. Fang, X. Y. Chen, S. F. Y. Li, H. B. Su, N.-J. Cho and H. Q. Zeng, *Chem. Sci.*, 2012, **3**, 2042–2046.
- 39 H. Q. Zhao, W. Q. Ong, X. Fang, F. Zhou, M. N. Hii, S. F. Y. Li, H. B. Su and H. Q. Zeng, *Org. Biomol. Chem.*, 2012, **10**, 1172–1180.
- 40 W. Q. Ong, H. Q. Zhao, C. Sun, J. E. Wu, Z. C. Wong, S. F. Y. Li, Y. H. Hong and H. Q. Zeng, *Chem. Commun.*, 2012, **48**, 6343–6345.
- 41 F. Zhou, H. L. Fu, W. Q. Ong, R. J. Ye, W. X. Yuan, Y.-J. Lu, Y.-P. Huo, K. Zhang, H. B. Su and H. Q. Zeng, *Org. Biomol. Chem.*, 2012, **10**, 5525–5528.
- 42 S. Guieu, A. K. Crane and M. J. MacLachlan, *Chem. Commun.*, 2011, **47**, 1169–1171.
- 43 Y. Hamuro, S. J. Geib and A. D. Hamilton, *Angew. Chem., Int. Ed. Engl.*, 1994, **33**, 446–448.
- 44 Y. Hamuro, S. J. Geib and A. D. Hamilton, *J. Am. Chem. Soc.*, 1997, **119**, 10587–10593.
- 45 Y. Hamuro, S. J. Geib and A. D. Hamilton, *J. Am. Chem. Soc.*, 1996, **118**, 7529–7541.
- 46 R. D. Parra, H. Q. Zeng, J. Zhu, C. Zheng, X. C. Zeng and B. Gong, *Chem.-Eur. J.*, 2001, **7**, 4352–4357.
- 47 J. Zhu, R. D. Parra, H. Q. Zeng, E. Skrzypczak-Jankun, X. C. Zeng and B. Gong, *J. Am. Chem. Soc.*, 2000, **122**, 4219–4220.
- 48 B. Gong, H. Q. Zeng, J. Zhu, L. H. Yuan, Y. H. Han, S. Z. Cheng, M. Furukawa, R. D. Parra, A. Y. Kovalevsky, J. L. Mills, E. Skrzypczak-Jankun, S. Martinovic, R. D. Smith, C. Zheng, T. Szyperski and X. C. Zeng, *Proc. Natl. Acad. Sci. U. S. A.*, 2002, **99**, 11583–11588.
- 49 V. Berl, I. Huc, R. G. Khoury, M. J. Krische and J. M. Lehn, *Nature*, 2000, **407**, 720–723.
- 50 V. Berl, I. Huc, R. G. Khoury and J.-M. Lehn, *Chem.-Eur. J.*, 2001, **7**, 2810.
- 51 H. Jiang, J.-M. Léger and I. Huc, *J. Am. Chem. Soc.*, 2003, **125**, 3448–3449.
- 52 Q. Gan, C. Y. Bao, B. Kauffmann, A. Grelard, J. F. Xiang, S. H. Liu, I. Huc and H. Jiang, *Angew. Chem., Int. Ed.*, 2008, **47**, 1715–1718.
- 53 Q. Gan, Y. Ferrand, C. Bao, B. Kauffmann, A. Grélard, H. Jiang and I. Huc, *Science*, 2011, **331**, 1172–1175.
- 54 J. L. Hou, X. B. Shao, G. J. Chen, Y. X. Zhou, X. K. Jiang and Z. T. Li, *J. Am. Chem. Soc.*, 2004, **126**, 12386–12394.
- 55 C. Li, S.-F. Ren, J.-L. Hou, H.-P. Yi, S.-Z. Zhu, X.-K. Jiang and Z.-T. Li, *Angew. Chem., Int. Ed.*, 2005, **44**, 5725–5729.
- 56 H. P. Yi, C. Li, J. L. Hou, X. K. Jiang and Z. T. Li, *Tetrahedron*, 2005, **61**, 7974–7980.
- 57 Z. Q. Hu, H. Y. Hu and C. F. Chen, *J. Org. Chem.*, 2006, **71**, 1131–1138.
- 58 Q. Yu, T. E. Baroni, L. Liable-Sands, A. L. Rheingold and A. S. Borovik, *Tetrahedron Lett.*, 1998, **39**, 6831–6834.
- 59 D. Kanamori, T. A. Okamura, H. Yamamoto and N. Ueyama, *Angew. Chem., Int. Ed.*, 2005, **44**, 969–972.
- 60 C. Tie, J. C. Gallucci and J. R. Parquette, *J. Am. Chem. Soc.*, 2006, **128**, 1162–1171.
- 61 X. Li, C. L. Zhan, Y. B. Wang and J. N. Yao, *Chem. Commun.*, 2008, 2444–2446.
- 62 This high level *ab initio* calculation along with the level of B3LYP/6-31G(d) have consistently enabled us to accurately predict the 3D topography of oligomers of varying types that were later experimentally verified by crystal structures, see ref. 29–31 and 34.
- 63 For similar oligomers made up of the identical repeating units as in pentamer 6, see ref. 56 and J.-L. Hou, H.-P. Yi, X.-B. Sha, C. Li, Z.-Q. Wu, X.-K. Jian, L.-Z. Wu, C.-H. Tung and Z.-T. Li, *Angew. Chem., Int. Ed.*, 2006, **45**, 796–800.
- 64 For a similar asymmetric binding of lithium and symmetric binding of potassium observed in the X-ray structures of Bell's sixfold symmetric torands, see: (a) T. W. Bell, P. J. Cragg, M. G. B. Drew, A. Firestone and D. I. A. Kwok, *Angew. Chem., Int. Ed. Engl.*, 1992, **31**, 345; (b) T. W. Bell, P. J. Cragg, M. G. B. Drew, A. Firestone and D. I. A. Kwok, *Angew. Chem., Int. Ed. Engl.*, 1992, **31**, 348.
- 65 HBTU is short for O-benzotriazole-N,N',N'-tetramethyl-uronium-hexafluoro-phosphate and BOP is short for benzotriazole-1-yl-oxy-tris-(dimethylamino)-phosphonium hexafluorophosphate.
- 66 S. S. Moore, T. L. Tarnowski, M. Newcomb and D. J. Cram, *J. Am. Chem. Soc.*, 1977, **99**, 6398–6405.
- 67 H. W. Wang and S. F. Sui, *J. Struct. Biol.*, 2001, **134**, 46–55.
- 68 K. Zhao and T. G. Mason, *Phys. Rev. Lett.*, 2009, **103**, 208302.
- 69 T. Schilling, S. Pronk, B. Mulder and D. Frenkel, *Phys. Rev. E*, 2005, **71**, 036138.
- 70 T. Bauert, L. Merz, D. Bandera, M. Parschau, J. S. Siegel and K.-H. Ernst, *J. Am. Chem. Soc.*, 2009, **131**, 3460–3461.
- 71 O. Guillermet, E. Niemi, S. Nagarajan, X. Bouju, D. Martrou, A. Gourdon and S. Gauthier, *Angew. Chem., Int. Ed.*, 2009, **48**, 1970–1973.
- 72 A. Durer, (1525) A Manual of Measurement of Lines, Areas and Solids by Means of Compass and Ruler [Facsimile Edition (1977) (Abaris Books, New York), translated with commentary by W. L. Strauss].
- 73 J. Kepler, (1619) Harmonices Mundi [Facsimile edition (1969) (Forni Editore, Bologna, Italy); Book II: On the Congruence of Harmonic Figures, English transl., J. V. Field (1979) Vistas Astron. 23, 109–141].
- 74 C. L. Henley, *Phys. Rev. B: Condens. Matter Mater. Phys.*, 1986, **34**, 797–816.
- 75 T. Tarnai, Z. Gaspar and L. Szalait, *Biophys. J.*, 1995, **69**, 612–618.
- 76 D. L. D. Caspar and E. Fontano, *Proc. Natl. Acad. Sci. U. S. A.*, 1996, **93**, 14271–14278.
- 77 G. Kuperberg and W. Kuperberg, *Discrete Comput. Geom.*, 1990, **5**, 389–397.

- 78 W. Feng, K. Yamato, L. Yang, J. S. Ferguson, L. Zhong, S. Zou, L. Yuan, X. C. Zeng and B. Gong, *J. Am. Chem. Soc.*, 2009, **131**, 2629–2637.
- 79 F. Li, Q. Gan, L. Xue, Z.-m. Wang and H. Jiang, *Tetrahedron Lett.*, 2009, **50**, 2367–2369.
- 80 Y. Liu, B. Qin and H. Q. Zeng, *Sci. China*, 2012, **55**, 55–63.
- 81 J. S. Ferguson, K. Yamato, R. Liu, L. He, X. C. Zeng and B. Gong, *Angew. Chem., Int. Ed.*, 2009, **48**, 3150–3154.
- 82 A. M. Zhang, Y. H. Han, K. Yamato, X. C. Zeng and B. Gong, *Org. Lett.*, 2006, **8**, 803–806.
- 83 Z. H. Wu, T. Hu, L. He and B. Gong, *Org. Lett.*, 2012, **14**, 2504–2507.
- 84 Y. H. Kim, J. Calabrese and C. McEwen, *J. Am. Chem. Soc.*, 1996, **118**, 1545.
- 85 F. J. Carver, C. A. Hunter and R. J. Shannon, *Chem. Commun.*, 1994, 1277–1280.
- 86 B. Qin, S. Shen, C. Sun, Z. Y. Du, K. Zhang and H. Q. Zeng, *Chem.-Asian J.*, 2011, **6**, 3298–3305.
- 87 B. Qin, C. Sun, Y. Liu, J. Shen, R. J. Ye, J. Zhu, X.-F. Duan and H. Q. Zeng, *Org. Lett.*, 2011, **13**, 2270–2273.
- 88 B. Qin, L. Y. Jiang, S. Shen, C. Sun, W. X. Yuan, S. F. Y. Li and H. Q. Zeng, *Org. Lett.*, 2011, **13**, 6212–6215.
- 89 Z. Y. Du, B. Qin, C. Sun, Y. Liu, X. Zheng, K. Zhang, A. H. Conney and H. Q. Zeng, *Org. Biomol. Chem.*, 2012, **10**, 4164–4171.